THE UNIVERSITY *of* EDINBURGH

The effect of stabilising mutations in β-catenin on PROTAC-mediated degradation kinetics

Evelina Gudauskaitė

MSc by Research in Genetics and Molecular Medicine

The University of Edinburgh

2024

SIGNED DECLARATION:

a) This thesis has been completed by Evelina Gudauskaitė (myself).
b) I have completed my master's as a member of the Wood laboratory, and I have worked under the supervision of Dr Brianda Hernandez-Moran and Dr Gillian Taylor, both postdoctoral scientists in the Wood laboratory. I have made a substantial contribution to the work presented, where I have included work completed solely by Dr Joe Marsh, I have made explicit reference to this in figure legends and text.
c) This work has not been submitted for any other degree or professional qualification.

Signature:

Date: 20.06.2024

ACKNOWLEDGEMENTS

I would like to thank members of the Wood laboratory, giving a special thanks to Dr Andrew Wood my primary supervisor, Dr Gillian Taylor and Dr Brianda Hernandez-Moran for all their supervision and assistance throughout the years.

I would also like to thank members of the Sequencing and Imaging Facility and the Flow Cytometry Unit at the Institute for Genetics and Cancer (University of Edinburgh) for their assistance in allowing me to generate the data presented in this report.

LAY ABSTRACT

In recent years, a new class of drugs called protein degraders has emerged, offering a promising approach to combatting diseases by breaking down harmful proteins within the body. These drugs, including PROteolysis TArgeting Chimeras (PROTACs), leverage our natural disposal system, the ubiquitin-proteasome system, to achieve their therapeutic effects. However, an important question remains unanswered: how does the natural breakdown rate of targeted proteins influence the effectiveness of PROTACs? To address this question, the study focused on β-catenin, a protein associated with cancer advancement when it becomes excessively active as a result of specific mutations. I conducted experiments to compare how different PROTAC drugs break down β-catenin with these cancer-causing mutations. Interestingly, β-catenin with mutations causing a fivefold increase in protein levels were broken down to the same extent as those without mutations. This observation highlights the robustness of PROTACs despite different protein levels. Understanding this could help to provide insights into the potential efficacy of PROTAC therapy across various cancer mutations in β-catenin and therefore help clinicians tailor treatment strategies for individual patients based on specific mutations.

ABSTRACT

Protein degrader drugs such as PROTACs have emerged as a chemical strategy to degrade pathological proteins via recruitment to E3 ubiquitin ligase complexes. How the basal rate of target protein turnover influences PROTAC-mediated degradation is incompletely understood. To address this question, I focused on the oncogenic transcription factor β-catenin, which is activated in human cancer by a variety of stabilising mutations within a degron motif. Here, I use a synthetic degron tag system to compare the kinetics of different PROTAC degraders on β-catenin activated via oncogenic stabilising mutations of different strengths. Interestingly, even an approximately fivefold increase in stability levels resulted in similar absolute protein levels after PROTACs-mediated degradation. This finding suggests that the maximum degradation was not solely determined by protein stability. Additionally, it showed that PROTACs can override natural rates of protein turnover, even when they have been disrupted by oncogenic mutations. Understanding this could help to predict how well patients with different oncogenic mutations will respond to PROTAC therapy.

TABLE OF CONTENTS

LIST OF FIGURES

LIST OF ABBREVIATIONS

APC: Adenomatous polyposis coli
ATTECs: Autophagy-targeting chimeras
Aux: Auxin
GFP: Green Fluorescent Protein
CRBN: Cereblon (E3 ligase)
VHL: Von Hippel-Lindau (E3 ligase)
c-Myc: cellular Myc
CK1: Casein kinase I
CRL: Cullin Ring E3 Ligase complex
CTNNB1: β-catenin
TPD: Targeted Protein Degradation
POI: Protein of Interest
PROTAC: Proteolysis Targeting Chimera
dTAG: Degradation Tag
AID: Auxin-Inducible Degron
DVL: Dishevelled
E1: Ubiquitin-activating enzyme
E2: Ubiquitin-conjugating enzyme
E3: Ubiquitin ligase
eGFP: Enhanced green fluorescent protein
EWS: Ewing sarcoma breakpoint region 1
FACS: Fluorescence-Activated Cell Sorting
WT: Wild-Type
FCS: Fetal Calf Serum
DMSO: Dimethyl sulfoxide
PBS: Phosphate Buffered Saline
FSC: Forward Scatter
SSC: Side Scatter
FLI: Friend leukaemia integration 1
GSK-3β: Glycogen synthase kinase-3β
IAA: indole-3-acetic acid
IAA: Indole-3-acetic acid
SCF: Skp1, Cullin, F-box containing complex
K-RAS: Kirsten rat sarcoma viral oncogene homolog
KIDINS220: Kinase D interacting substrate 220
LB: L-Broth
LRP5/6: Low-density lipoprotein receptor-related protein
LYTACs: Lysosome-targeting chimeras
MMPs: matrix metalloproteinases
PRKRA: Protein activator of interferon-induced protein kinase
PROTACs: Proteolytic targeting chimeras
TCF/LEF: T-cell factor/lymphoid enhancer-binding factor
tTPD: tag-targeted protein degrader
UPS: ubiquitin-proteosome system
VPS4A: Vacuolar Protein Sorting 4A
Wnt: Wingless-type MMTV integration site family

1. INTRODUCTION

1.1. Protein Turnover

Proteins are continuously being synthesised and degraded; a process called protein turnover (Hinkson and Elias, 2011). Protein turnover maintains proteostasis by ensuring that functional proteins are maintained at the correct concentrations and proper locations for cellular activities. Simultaneously, it ensures that misfolded, aged, or damaged proteins are eliminated (Labbadia and Morimoto, 2015). There are several cellular surveillance systems responsible for protein turnover. Protein production by mRNA translation is driven by the ribosome, and controlled through various mechanisms, including regulatory proteins, RNA-binding factors, and post-transcriptional modification (Gerstberger et al., 2014; Tahmasebi *et al.*, 2019). While protein degradation is controlled by the lysosome and proteasome. In lysosomal proteolysis, proteins are engulfed by membrane-enclosed vesicles (e.g., autophagosomes), which then fuse with lysosomes that degrade protein with endogenous digestive enzymes (Huber and Teis, 2016). The ubiquitin-proteosome system (UPS) degrades proteins via several enzymatic steps. Initially, ubiquitin undergoes activation by ubiquitin-activating enzyme (E1). Subsequently, ubiquitin is transferred to a ubiquitin-conjugating enzyme (E2) and ultimately attached to the substrate protein by a ubiquitin ligase (E3). The ubiquitin ligase recognises specific motifs, called 'degrons' in the targeted protein. Additional ubiquitin molecules are then conjugated onto the first ubiquitin that is attached to the targeted protein, creating a polyubiquitinated chain. This complex is identified by the 26S proteasome, triggering targeted protein degradation (Adams, 2003). The changes in protein turnover can occur due to physiological stimuli, development and ageing, and diseases (Labbadia and Morimoto, 2015). Understanding this protein turnover change can provide supplementary information when developing therapies (AlQahtani et al., 2019; Ross et al., 2021).

1.2. Degron

Most degrons identified within endogenous proteins (referred to hereafter as the 'native' degron') are short linear motifs that are predominantly located in proximity to post-translational modification sites and within disordered protein regions (Xu et al., 2023). Native degrons serve as specific signals recognised by E3 ligases to modulate protein turnover through the UPS. Regulation of native degrons occurs through various mechanisms. Misfolded or damaged proteins reveal degrons that would otherwise be concealed within the protein structure (Lucas and Ciulli, 2017). Some post-translational modifications occur in the absence of stimuli; for instance, when the Wnt pathway is inactive, phosphorylation occurs, activating the degron in β-catenin. Similarly, under normoxic conditions, hypoxia-inducible factor (HIF-1) exhibits a constitutively hydroxyl-activated degron, signalling for degradation (Lee *et al.*, 2023). In plants, the abundance indole-based hormones of the auxin family induces degradation of the Aux/IAA family of transcriptional repressors by modulating the E3 and degron interactions (Tan *et al.*, 2007). Mutations that disturb the regulation of degron functionality can interfere with the control of protein turnover. This disruption may lead to the misplacement of proteins intended for degradation and frequently contributes to pathological conditions (Mészáros *et al.*, 2017; Hou *et al.*, 2022).

1.3. Targeted Protein Degradation

Targeted protein degradation (TPD) technology has surfaced as a promising therapeutic strategy. Various TPD strategies have been developed such as proteolytic-targeting chimeras (PROTACs) (Zou, Ma and Wang, 2019), molecular glues (Besten and Lipford, 2020), lysosome-targeting chimeras (LYTACs) (Banik *et al.*, 2020), autophagy-targeting chimeras (ATTECs) (Li *et al.*, 2020), many other systems (Song *et al.*, 2023). TPDs offer several advantages over traditional small-molecule inhibitors. They have the potential to target proteins previously considered "undruggable", including transcription factors, due to their unique mode of action. TPDs reduce the required dosage by not relying on target saturation, preventing potential toxic effects. They can bind to multiple sites within the protein, extending beyond well-defined catalytic sites. Removal of proteins by TPD can perturb scaffolding functions in a way that is not achievable by inhibition (Kelm *et al.*, 2023; Song *et al.*, 2023). Currently, more than 20 PROTACs and over 10 molecular glues are undergoing clinical trials, highlighting the growing interest and potential of this approach in the drug development (Békés et al., 2022; Ciulli et al., 2023). TPD can also facilitate functional genomic and proteomic studies and design disease models (Macdonald et al., 2022). Fast degradation avoids molecular compensation and cellular adaptation, allowing the identification of direct protein functions (Wu et al., 2020). Potentially overcoming the limitations of genetic perturbation strategies (e.g., CRISPR–Cas9 or RNA interference), which can take days to remove the protein function. The reversibility and titration of the targeted depletion can help to determine critical time points of disease progression and when therapeutic interventions could yield clinical benefit (Natsume and Kanemaki, 2017).

1.4. PROTACs & Molecular Glues

The two most widely used TPDs that harness UPS systems are molecular glues and PROTACs. Molecular glues (e.g., lenalidomide and auxin-inducible degron (AID)) are monovalent, binding to either the target protein or the E3 ligase. This binding promotes the formation of a novel surface interface that stabilises the interaction between the target protein and E3 ligase, leading to degradation. Having a relatively low molecular weight, glues are expected to have higher membrane permeability and better cellular uptake, therefore improved bioavailability (Benet *et al.*, 2016; Che *et al.*, 2018). The challenge lies in the identification of molecular glues. Many ligands have been discovered not through rational screening but by serendipity following phenotypic screening. However, the focus is now shifting towards rational screening methods for molecular glues (Holdgate *et al.*, 2023).

PROTACs are bivalent degraders i.e. composed of two distinct chemical moieties joined by a covalent linker. This design allows them to independently interact with E3 ligase and target protein. PROTACs usually have larger molecular weights, leading to challenges in delivery and bioavailability. (Neklesa, Winkler and Crews, 2017; Simpson *et al.*, 2020). PROTAC's degradation potency can be negatively impacted in high concentrations, where binding sites in the target protein and E3 ligase become saturated and only form PROTAC dimers, without forming a ternary complex.

This is known as the 'hook effect' (Kostic and Jones, 2020). The schematic representation of PROTACs is shown in Figure 1.

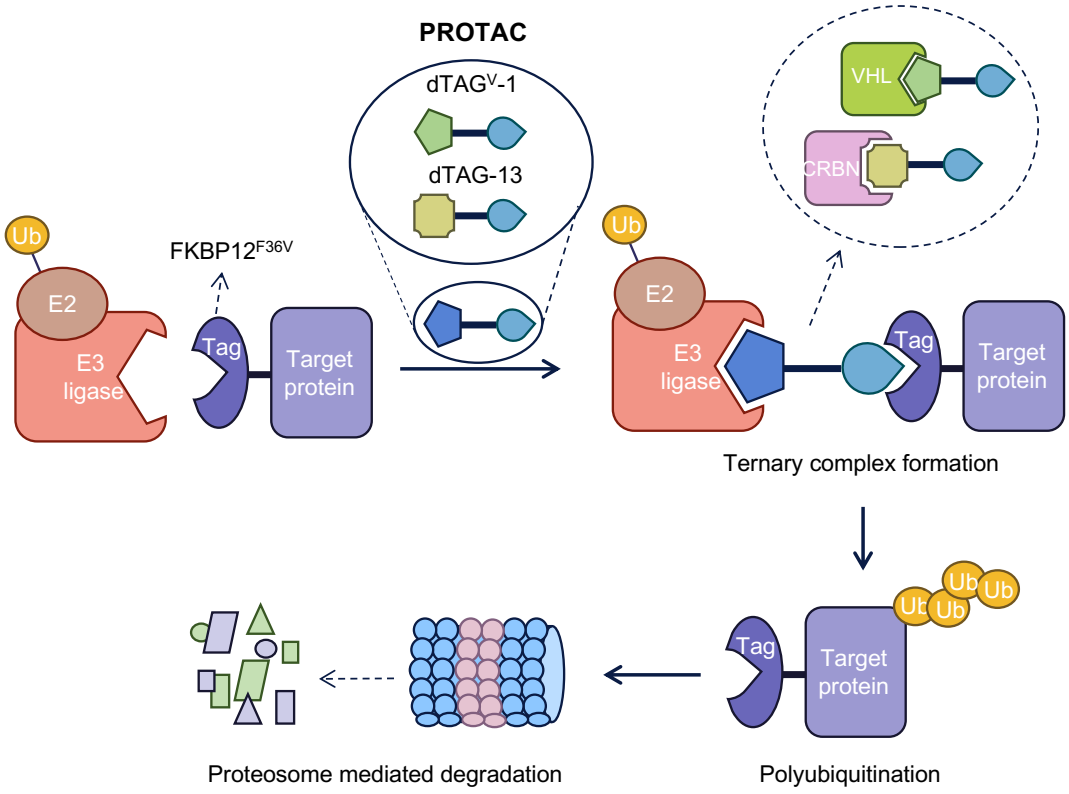

Figure 1 Mechanism of PROTAC-mediated degradation of FKBP12^{F36V}-tagged target proteins. The target protein is fused with a synthetic tag (FKBP12^{F36V}), which specifically recruits ligands such as dTAG^{V}-1 and dTAG-13. PROTACs (heterobifunctional molecules) independently bind to the E3 ubiquitin ligase and the FKBP12^{F36V}-tagged target protein. dTAG^{V}-1 binds to the VHL E3 ligase, while dTAG-13 binds to the CRBN E3 ligase. The simultaneous binding of the PROTAC to the target protein and the E3 ligase forms a ternary complex. The E3 ligase ubiquitinates the target protein within the ternary complex. The polyubiquitinated target protein is recognised and degraded by the proteasome, leading to a reduction in the levels of the target protein in the cell.

The human genome encodes more than 600 E3 ubiquitin ligases; however, only a limited number of E3 ligases have been effectively utilized. Among the most employed are the Cullin Ring Ligases (CRLs) CRL2^{VHL}, where the PROTAC binds to the von Hippel-Lindau (VHL) substrate receptor, and CRL^{CRBN} , where the cereblon (CRBN) substrate receptor of CRL4A^{CRBN} is bound. "Undruggable" transcription factors like IKZF1/3 have been demonstrated to undergo degradation when exposed to molecular glues such as lenalidomide, thalidomide, or pomalidomide, all inducing the formation of a ternary complex with CRBN (Sasso *et al.*, 2023). Ligands such as HaloPROTAC recruits CRL2^{VHL} to the HaloTag (Buckley *et al.*, 2015) and TAG-based PROTACs ligands such as dTAG^{V}-1 recruit VHL, or dTAG-13 recruit CRBN (Simpson *et al.*, 2022). Notably, distinct degradation efficiencies were observed; dTAGV-1 effectively degraded the oncogenic transcription factor K-RAS GTPase and EWS/FLI, while dTAG-13 did not exhibit the same efficacy (Bond *et al.*, 2020; Nabet *et al.*, 2020; Zeng *et al.*, 2020). In contrast, oncogenic tyrosine kinase BCR-ABL was degraded with CRBN-recruiting PROTACs more efficiently than VHL recruiters (Lai *et al.*, 2016). The observed variations in degradation efficiency may be attributed to differences in the abundance or subcellular distribution of both the E3 ligase and the targeted protein (Zhang *et al.*, 2019), or to different efficiencies of ubiquitin transfer arising from spatial

configuration of the distinct ternary complexes (Buetow and Huang, 2016). Therefore, selecting a specific E3 ligase for recruitment holds the potential to enhance both the efficiency and specificity of degradation.

1.5. Degron Tagging

TPD strategies have two distinct approaches for protein targeting. The first involves direct targeting of the protein, which requires in-depth knowledge of the target, ligand optimisation and validation. Alternatively, a more streamlined strategy fuses a known degron tag with the target protein. Various types of these degron tags exist, such as AID, which originates from a natural degron. In this context, plant hormones like auxins (e.g., indole-3-acetic acid (IAA)) engage with the TIR1 protein (Transport Inhibitor Response 1), increasing affinity for the target protein containing the degron (Natsume *et al.*, 2016). Another example is the BromoTag ($Brd4^{BD2\ L387A}$), which functions as part of the "Bump-and-Hole"–PROTAC System (Bond *et al.*, 2021). dTAG system uses an $FKBP12^{F36V}$ tag, the same tag can engage with various heterobifunctional ligands that can facilitate degradation through different E3 complexes (Nabet *et al.*, 2018).

A clear drawback of tag fusion is the potential disruption of protein expression, localisation, and function. Commonly, tags are fused at the N- or C-terminus, however, the success is highly target-dependent, encompassing both the specific construct design and the technology used, affecting protein expression and degradation. Some targets were found to be highly degradable when tagged at the N- or C-termini with different technologies (e.g., VPS4A and PRKRA), while others, KIDINS220 for example, were only degradable when tags were fused to the N-terminus and degraded using dTAG or IKZF3d system (Bondeson et al., 2022). When fusion to the N- or C-termini is not possible, proteins can be tagged internally (Zordan *et al.*, 2015). Several techniques can be used to determine optimal internal tagging positions such as the Saturated Programmable Insertion Engineering (SPINE) (Coyote-Maestas *et al.*, 2020) and the transposon technology (Nadler *et al.*, 2016). While computational tools can offer valuable predictions for potential optimal sites, it's important to note that there is limited availability of tools that have undergone comprehensive experimental verification. Dr Joe Marsh (MRC HGU) has developed a computational tag insertion prediction tool, which retrieves amino acid sequences from homologous proteins across species and performs pairwise alignments, identifying sites at which amino acid insertions have occurred naturally during evolution. Longer insertions are given more weight according to log(L), where L is the length of the insertion in amino acids. Sites that have 'tolerated' evolutionary insertions are predicted to be more tolerant, on average, to artificial insertions. However, the tool is untested, so we do not know how well it performs in practice.

1.6. β-Catenin and Wnt Pathway

Wnt signalling controls the growth and patterning of diverse tissues during development, and homeostasis of adult tissues such as the intestine and liver. The Wnt signalling pathways include noncanonical and canonical pathways. The noncanonical Wnt pathways operate independently from β-catenin and T-cell factor/lymphoid enhancer-binding factor (TCF/LEF). While the canonical Wnt pathway, also known as the Wnt/β-catenin pathway, includes the nuclear translocation of β-catenin and activation of target genes via TCF/LEF transcription factors (Clevers, 2006).

The human β-catenin (CTNNB1) protein consists of 781 amino acids and is divided into 3 domains. The central domain of 138-664 residues are armadillo repeats, which is a relatively rigid scaffold that can serve as an interaction platform for binding proteins to β-catenin in the membrane, cytosol and nucleus. The N-terminal and C-terminal domains are structurally flexible (Huber *et al.,* 1997). β-catenin is a bifunctional protein that has transcriptional and adhesive properties. The N-terminal domain of β-catenin connects the β-catenin/E-cadherin complex to the α-catenin, which then anchors the junction to the cytoskeleton. Therefore, β-catenin is a central component of adherence junctions, without which junctions lose their tension and structure (Rimm *et al.*, 1995; Xing *et al.*, 2008; Van Der Wal and Van Amerongen, 2020).

The β-catenin-dependent Wnt signalling pathway can be broken down into 4 components: the extracellular signal, membrane receptors, cytoplasmic signal transduction, and nuclear. Extracellular signals are mostly facilitated by Wnt ligands, including Wnt1, Wnt3a and Wnt5a. Wnt ligand binds to the transmembrane co-receptors Frizzled and low-density lipoprotein receptor-related protein (LRP5/6). Upon activation, Frizzled activates cytoplasmic Disheveled (DVL) protein, which then inhibits the formation of β-catenin destruction complex that consists of glycogen synthase kinase-3β (GSK-3β), AXIN, adenomatous polyposis coli (APC), and casein kinase I (CK1). Therefore β-catenin stabilises and translocates to the nucleus, where it binds to TCF/LEF and activates the transcription of target genes such as matrix metalloproteinases (MMPs) and c-Myc. When the Wnt pathway is inactive, the destruction complex captures cytosolic β-catenin, GSK-3β and CK1 phosphorylates N-terminus of β-catenin, resulting in phosphorylated β-catenin recognition by the β-TrCP ubiquitin ligase and degradation by UPS (Wu *et al.*, 2003; Liu *et al.*, 2022). Schematic representation of the Wnt pathway is displayed in Figure 2.

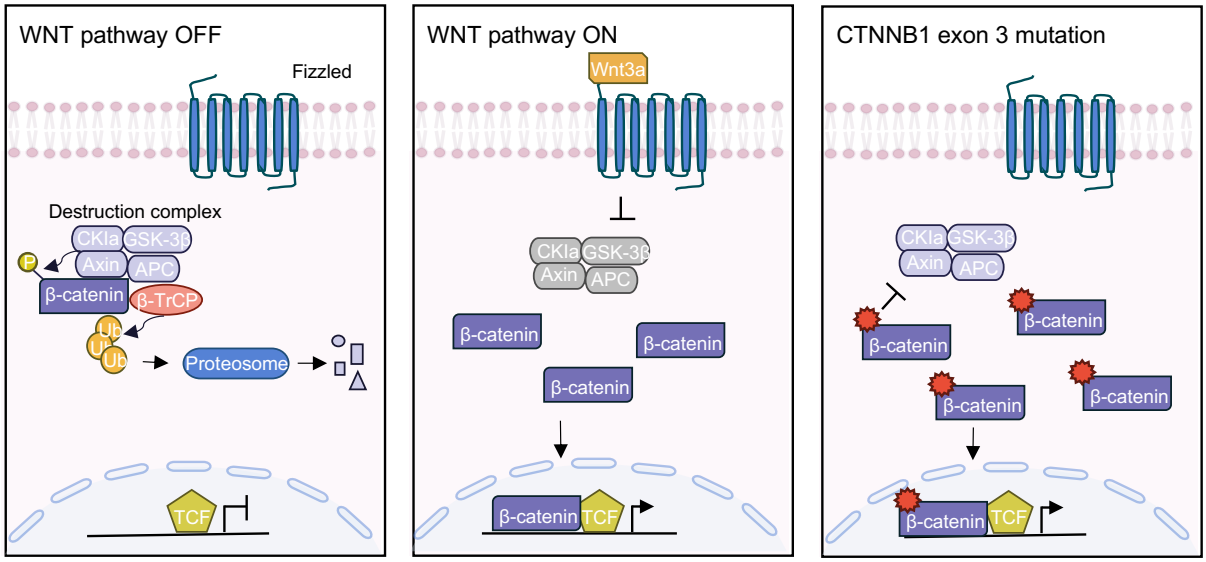

Figure 2 Mechanism of the WNT pathway and β-catenin regulation. WNT Pathway OFF: In the absence of WNT signalling, the destruction complex, consisting of CKIα, GSK3β, AXIN, and APC, phosphorylates β-catenin. Phosphorylated β-catenin is ubiquitinated by the SCFβTrCP complex, leading to its proteasome-mediated degradation. WNT Pathway ON: Upon activation by a WNT ligand such as Wnt3a, the formation of the destruction complex is inhibited. This inhibition prevents the degradation of β-catenin, allowing it to accumulate in the cytoplasm. Accumulated β-catenin is then translocated to the nucleus, where it initiates the transcription of WNT target genes. CTNNB1 Exon 3 Mutation: Mutations in exon 3 of β-catenin affect the native degron, impairing the efficiency of the destruction complex. This impairment leads to the accumulation of β-catenin and its translocation to the nucleus, where it initiates WNT target gene transcription.

Aberrant activation of the Wnt signalling pathway results in various types of cancer. This is often caused by mutations disrupting the destruction complex, such as APC (Schatoff *et al.*, 2019), AXIN (Yardy *et al.*, 2009) or deletion in GSK-3β (Guezguez *et al.*, 2016). However gain of function mutations in β-catenin are very common in particular tumour types such as hepatocellular and endometrial carcinoma, and localise within a native degron in exon 3, responsible for the $SCF^{\beta TrCP}$-mediated degradation (Mészáros *et al.*, 2017; Gao *et al.*, 2018). Mutational scanning of the β-catenin hot spot region in exon 3 revealed high and low effect mutations, which activated downstream signalling to different degrees (Rebouissou *et al.*, 2016; Krishna *et al.*, 2023), presumably via elevating β-catenin protein levels.

2. AIMS

In my project, I will be trying to answer the following questions:

2.1. How do synthetic degrons fused at different positions of β-catenin affect normal expression and turnover?

I will develop a model system to study the degradation of β-catenin. I will assess the expression of tagged β-catenin at various positions in the steady state, and check whether the synthetic degron influences normal mechanisms of protein turnover in the non-induced state. Additionally, I will compare the kinetics of degradation in these constructs following the recruitment of different E3 ligases.

2.2. Does the mechanism of oncogene activation affect the degradation maximum?

I will assess whether exon 3 mutations that stabilise β-catenin to different extents influence PROTAC-mediated degradation kinetics.

3. MATERIALS AND METHODS

3.1. Construct Design, Synthesis and Cloning to Expression Vector

3.1.1. Construct Design and Synthesis

The coding sequences of the β-catenin transcript (ENST00000349496.1), the $FKBP12^{F36V}$ (NCBI: LC087168.1), and the eGFP (NCBI: MG736726.1) were used to design constructs. Three combinations of constructs were designed: β-catenin – $FKBP12^{F36V}$ – eGFP, eGFP – $FKBP12^{F36V}$ – β-catenin and β-catenin internal $FKBP12^{F36V}$ – eGFP (Figure 4a). All constructs were connected through flexible linker GGGGS (x3). The internal tag position was based on Dr Joe Marsh's computational tool result (Figure 4b). These constructs were ordered to be synthesised as clonal genes in pTwist Amp High Copy Cloning Vector by TWIST Bioscience. Gene fragments containing either S33F, T41A and S45F mutations in β-catenin were synthesised by TWIST Bioscience.

3.1.2. Construct Cloning to Expression Vector

Expression vector pCDNA5-CAG-FRT (Ford *et al.*, 2018) and clonal gene constructs were subjected to restriction enzyme digestion with NheI-HF and KpnI-HF enzymes overnight at 37 °C, followed by 1% agarose gel electrophoresis, where corrected size bands were cut-out of the gel and subjected to gel extraction according to the standard protocol of the QIAquick Gel Extraction Kit (Catalog no.: 28706X4). The Ligation (ratio of 3:1 (insert: vector)) was set overnight at 4 °C with T4 DNA ligase based on the manufacturer's instructions (Promega, Part# 9PIM180) and transformed into *Escherichia coli (E. coli)* Library Efficiency DH5α Competent Cells (Catalog no.: 18263012) as per standard protocol. Single colony then inoculated in Luria – broth (LB) media with 100 μL/mL of ampicillin and incubated overnight at 37 °C whilst shaking. QIAprep Spin Miniprep Kit (Catalog no.: 27104 and 27106) was used for plasmid purification from overnight bacterial inoculation the following day.
Gene fragments containing either S33F, T41A and S45F mutations in β-catenin were first cloned into Zero Blunt TOPO PCR Cloning Kit (Catalog no.: 450245) and transformed into DH5α competent cells, inoculated, and purified (as above). Then purified plasmid were subjected to restriction enzyme digestion with NheI-HF and Bsu36I or AflII enzymes overnight at 37 °C, followed by the same sequence of events as clonal gene.

3.2. Stable Cell Line Generation

Each pCDNA5-CAG-FRT expression vector containing different β-catenin constructs were integrated into the same genomic landing pad in T-REx HeLa and T-REx HEK 293 cells (Catalog no.: R71407 and R78007) cells via Flp recombinase-mediated DNA recombination at the FRT site (ThermoFisher, 2024), schematic representation shown in Figure 3. This resulted in the integration of the full plasmid, such that each β-catenin construct is driven by the same promoter, at the same genomic location. Lipofectamine 3000 (Catalog no.: L3000001) was used for transfection to the standard protocol. Cells were selected with hygromycin B, and then GFP-positive cells were isolated via Fluorescence-Activated Cell Sorting (FACS) and used without clonal expansion from single cells. T-REx HeLa and Flp-In T-REx 293 cell lines were cultured in complete Dulbecco′s Modified Eagle′s Medium (DMEM) (Sigma-Aldrich, D5796) supplemented with 10% Fetal Calf Serum (FCS) (IGC Technical Services) and 1% Penicillin-Streptomycin solution (P 70 mg/l, S 130 mg/l, IGC Technical Services). All cells were incubated at 37°C, 5% CO_2 and a humidified atmosphere. Cells were split and passaged once around 80% confluency was reached.

3.3. Steady-State Expression

Trypsinised stable cell lines were analysed using flow cytometry (CytoFLEX S) to quantify GFP fluorescence. The data was processed using FlowJo 10, and the mean GFP fluorescence for each sample was determined by subtracting the mean autofluorescence value from equivalently gated GFP negative cells. The steady-state

expression results were displayed as a boxplot, generated by R, using Dr Gillian Taylor's (postdoctoral scientist in the Wood laboratory) script.

Site specific recombination using FLP-In system

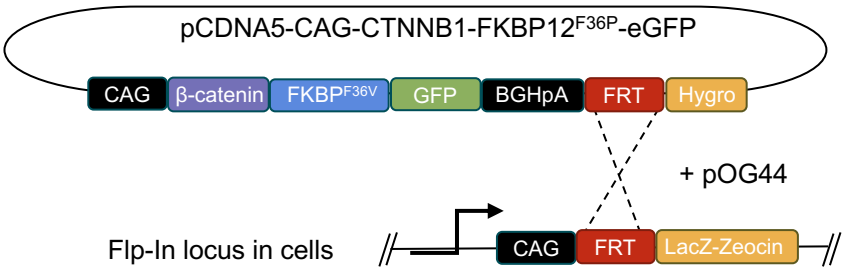

Figure 3 Site specific recombination using the Flp-In system**.** The Flp-In system employs Flp recombinase to achieve the integration of an expression vector into a predetermined genomic location with the presence of a single Flp Recombination Target (FRT) site. The expression vector, carrying a matching FRT site, is co-transfected with a plasmid encoding Flp recombinase (pOG44). Flp recombinase facilitates the recombination between the FRT sites on the host genome and the vector, resulting in site-specific integration of the gene of interest.

3.4. Dose-Response and Time-Dependant Degradation

3.4.1. Dose-response

Serial dilutions of dTAG^{V}-1 and dTAG-13 were done to achieve the following concentrations 1 μM, 500 nM, 100 nM, 50 nM, 10 nM, 5 nM, 1 nM, 0.1 nM, 0.01 nM, 0.001 nM and were dispensed onto a day prior plated cell (4 x 10^4) with C-terminally and internally tagged β-catenin. After 2 hours of incubation at 37 °C, cells were washed and trypsinised for flow cytometry to quantify GFP fluorescence. Cells were kept on ice until analysis.

3.4.2. Dose-response with Cycloheximide

100 μg/mL of cycloheximide (CHX) was dispensed onto a day prior plated cell (4 x 10^4) with serial dilutions of dTAG^{V}-1 with following concentrations 1 μM, 500 nM, 100 nM, 50 nM, 10 nM, 5 nM, 1 nM, 0.1 nM, 0.01 nM, 0.001 nM, which were treated for 2 h. After 2 hours of incubation at 37 °C, cells were washed and trypsinised for flow cytometry to quantify GFP fluorescence. Cells were kept on ice until analysis. Analysis was conducted as described in Section 3.5 for only dTAG^{V}-1 samples, while with the correction for CHX (+dTAG^{V}-1) performed using an equivalent cell line treated with CHX only.

3.4.3. Time-Dependant Degradation

A day prior plated cells with C-terminally tagged β-catenin were treated with dTAG^{V}-1 at a concentration of 100 nM at specific timepoints: 0.5 h, 1 h, 2 h, 4 h, 6 h and 24 h and incubated at 37 °C, cells then processed as described above.

3.5. Degradation Analysis

The data was analysed using FlowJo 10, and the mean GFP fluorescence for each sample was determined by subtracting autofluorescence from GFP negative cells. Then corrected fluorescence of the degrader-treated samples was normalised to 100% by dividing the corrected fluorescence of the sample by the corrected fluorescence of the untreated sample and multiple by 100%. Corrected fluorescence and normalised results were displayed as a dose-response curve, generated by R, using Dr Brianda Hernandez-Moran (postdoctoral scientist in the Wood laboratory) script. The degradation maximum (D_{max}) was determined by subtracting the percentage of remaining protein from 100 %, selecting the highest percentage observed at any given concentration or timepoint. The half-maximal degradation concentration (DC_{50}) was determined using the built-in model function in R for effective dose (ED) at 50% response.

3.6. Post Degradation Recovery

A day prior plated cells (1.5×10^4) with C-terminally tagged β-catenin were treated with $dTAG^V$-1 at a concentration of 100 nM for 24 h. Then, media with $dTAG^V$-1 was aspirated and cells were washed 3 times with PBS. Fresh media was added and left for further incubation at 37 °C. When cells confluency reached ~ 90%, cells were transferred into 12 or 6-well plates. Cells then were trypsinised and analysed by flow cytometry to quantify GFP fluorescence. The obtained data was normalised as above.

3.7. Whole Cell Protein Lysate and Western Blot

The day prior plated HeLa cells were treated with $dTAG^V$-1 at a concentration of 200 nM. Untreated cells were included as a control. After 2 h incubation at 37 °C cells were trypsinised and cell pellet washed with PBS. Alternatively, cells at the steady state were trypsinised and cell pellet washed with PBS.

The cell pellet was lysed with RIPA lysis buffer (50 mM Tris-HCl (pH 8), 150 mM NaCl, 1% NP-40, 0.5% Na-deoxycholate, 0.1% SDS, 1:100 protease inhibitor cocktail) on ice for 30 min, and protein lysate was quantified with the BCA assay. 10 – 20 μg of protein was loaded and separated in the 4-12% Bis-Tris gel using 1X MOPS running buffer, run at 100 V for 90 min. The gel was then wet transferred using Genie Blotter with transfer buffer (25 mM Tris, 200 mM glycine, 20% methanol, 0.02% SDS) on the 100% methanol pre-soaked membrane at 12 V for 90 min. The membrane was blocked by 5% milk powder (Marvel) in Tris Buffered Saline (TBS) with 0.1% Tween 20. The membrane was probed with primary antibodies either anti-GFP (1:500 or 1:1000) or anti-CTNNB1 (1:2000) (for loading control anti-H3 (1:100,000), anti-tubulin (1:1000) or anti-GAPDH (1:400)) diluted in block solution. The membrane was washed in TBS-Tween 20 solution (three washes × 10 min). HRP-conjugated secondary antibodies were also diluted in the block solution (anti-mouse (1:2500) or anti-rabbit (1:5000)), followed by washes. Western Blot was then developed under ImageQuant LAS 4000.

3.8. Cycloheximide (half-life) chase assay

HEK293 cells were plated the day prior to treatment with cycloheximide (CHX) at a concentration of 100 μg/mL for varying durations: 6, 8, and 16 hours. Following treatment, cells were trypsinised, lysed, and subjected to Western blot analysis as

described previously. Western blot bands were quantified using ImageJ software. The density of each band was measured, representing the sum of the pixel values within the selected area, hence the protein abundance. Then the density of sample was normalised to loading control (i.e., tubulin). This was done by dividing sample density by corresponding loading control band density. Subsequently, the normalised values were converted into percentages relative to the vehicle-treated sample, which was set as 100%. To determine the protein's half-life, an exponential decay model was fitted to the normalised data using R software. From the decay constant (k) obtained from the model, the protein's half-life ($t_{1/2}$) was calculated using the formula $t_{1/2}=\ln(2)/k$.

3.9. Immunocytochemistry

Cells were plated on a coverslip in a 6-well plate a day prior. On the day, cells were washed with PBS containing calcium and magnesium (PBS++), followed by fixation with ice-cold 4% formaldehyde for 10 minutes. After fixation, cells underwent three washes with PBS++. Permeabilization was performed for 10 minutes in PBS containing 0.2% Triton X100, followed by additional washes. The cells were then blocked in 0.3% BSA in PBS for 1 hour and incubated with anti-tubulin and GFP-booster Alexa Fluor 488 (green) for an additional 1 hour. After the washing step, the coverslip was incubated with anti-rabbit Alexa Fluor 555 (red) for 1 hour, followed by another round of washing before DAPI (blue) staining for 5 minutes. Finally, coverslips were mounted onto slides, and imaged using confocal microscopy. Image analysis was performed with CellProfiler, using segmentation techniques, where cytoplasm was set as a larger object and nucleus as smaller, which was extracted when quantifying the fluorescence of cytoplasm. This method enabled precise quantification of fluorescence across a minimum of 550 cells.

3.10. Wnt Pathway Activation

C-terminally tagged β-catenin stable cell lines were treated with GSK-3β inhibitor (CHIR99021) for 24 h at a concentration of 10 nM. Cells were washed with PBS and trypsinised for flow cytometry to quantify GFP fluorescence. The data was processed using FlowJo 10, and the mean GFP fluorescence for each sample was determined by subtracting autofluorescence from GFP negative cells. The tagged protein expression results were displayed as a boxplot, generated by R, using Dr Gillian Taylor’s (postdoctoral scientist in Wood laboratory) script.

3.11. RT-qPCR

Total RNA was isolated from cell pellets of C-terminally tagged β-catenin stable cell lines using TRIzol reagent, following the manufacturer’s protocol. Subsequently, the RNA underwent DNA removal using the DNA-Free kit (Invitrogen) to eliminate any DNA contaminants. The RNA was then reverse transcribed into complementary DNA (cDNA) using the RevertAid H Minus First Strand cDNA Synthesis Kit (Thermo Fisher Scientific). Primer pairs targeting Axin 2 (NM_004655) and β-Actin (NM_001101), sourced from OriGene, were employed for quantitative polymerase chain reaction (qPCR). SYBR Select Master Mix protocol was utilized for qPCR, according to the manufacturer’s instructions, with amplification performed on the Bio-Rad CFX96 Touch instrument. The qPCR cycling conditions consisted of an initial activation step

at 95°C for 5 min, followed by 39 cycles of denaturation at 95°C for 10 sec, annealing at 55°C for 10 sec, and extension at 72°C for 20 sec, with data acquisition at each step. A melting curve analysis was conducted with a temperature profile of 95°C for 10 sec, 65°C for 5 sec, and subsequent reduction by 0.5°C increments from 95°C.
To evaluate the relative change in gene expression between cell lines expressing transgenic tagged β-catenin and those with wild-type β-catenin, the delta-delta Ct (ΔΔCt) method was employed. This method involved determining the difference in threshold cycle (Ct) values between the target gene (Axin 2) and the reference gene (β-Actin) for each sample. The Ct values of the target gene were then normalized to those of the reference gene to obtain the ΔCt. The ΔΔCt was then calculated by subtracting the ΔCt value of the control sample from the ΔCt value of each sample. Finally, the relative change in gene expression between the experimental and control conditions was determined using the formula 2^(-ΔΔCt).

3.12. Computational 3D Protein Model

3D protein models were generated using AlphaFold2 using the primary amino acid sequence of each construct to generate a PDB file. Models were displayed using ChimeraX. ChimeraX function MatchMaker was employed to superimpose two protein structures, wild-type β-catenin compared to tagged β-catenin, to produce Root Mean Square Deviation (RMSD).

4. RESULTS

4.1. Evaluating Steady-State Expression and Degradability Kinetics of Tagged β-Catenin in N-, C-terminal or Internal Fusions

Constructs containing β-catenin, $FKBP12^{F36V}$ tag and eGFP reporter were connected with flexible GGGGS (x3) linker, fused at N-, C-terminal or internally (Figure 4a). The internal tag position was based on Dr Joe Marsh's tolerable position prediction tool, which indicated a high-scoring position between 551 and 552 amino acids, as highlighted in Figure 4b. AlphaFold2 generated 3D models of these constructs, which then were used to evaluate the similarity of generated 3D structure between wild-type (Figure 4c) and tagged β-catenin (Figure 4d-f). ChimeraX function MatchMaker was used to superimpose two protein structures, providing an RMSD score that measures the average distance between the atoms of superimposed structures (Brüschweiler, 2003), this way allowing to assess the degree to which tags are predicted to modify the structure of tagged compared to untagged β-catenin. All RMSD were below 1 Å, indicating a high degree of structural similarity despite the fused tag (Figure 4d-f).

To evaluate the effect of tag position on the steady-state expression of β-catenin in cells, GFP fluorescence was quantified via flow cytometry. Stable cell lines using the Flp-in system were generated. High levels of fluorescence were observed in cells with N-terminal tag, while C-terminal and internal tag fusions had lower fluorescence in both HeLa and HEK293. There was a slight difference in fluorescence between C-terminal and internal fusions among cell lines (Figure 5a-b).

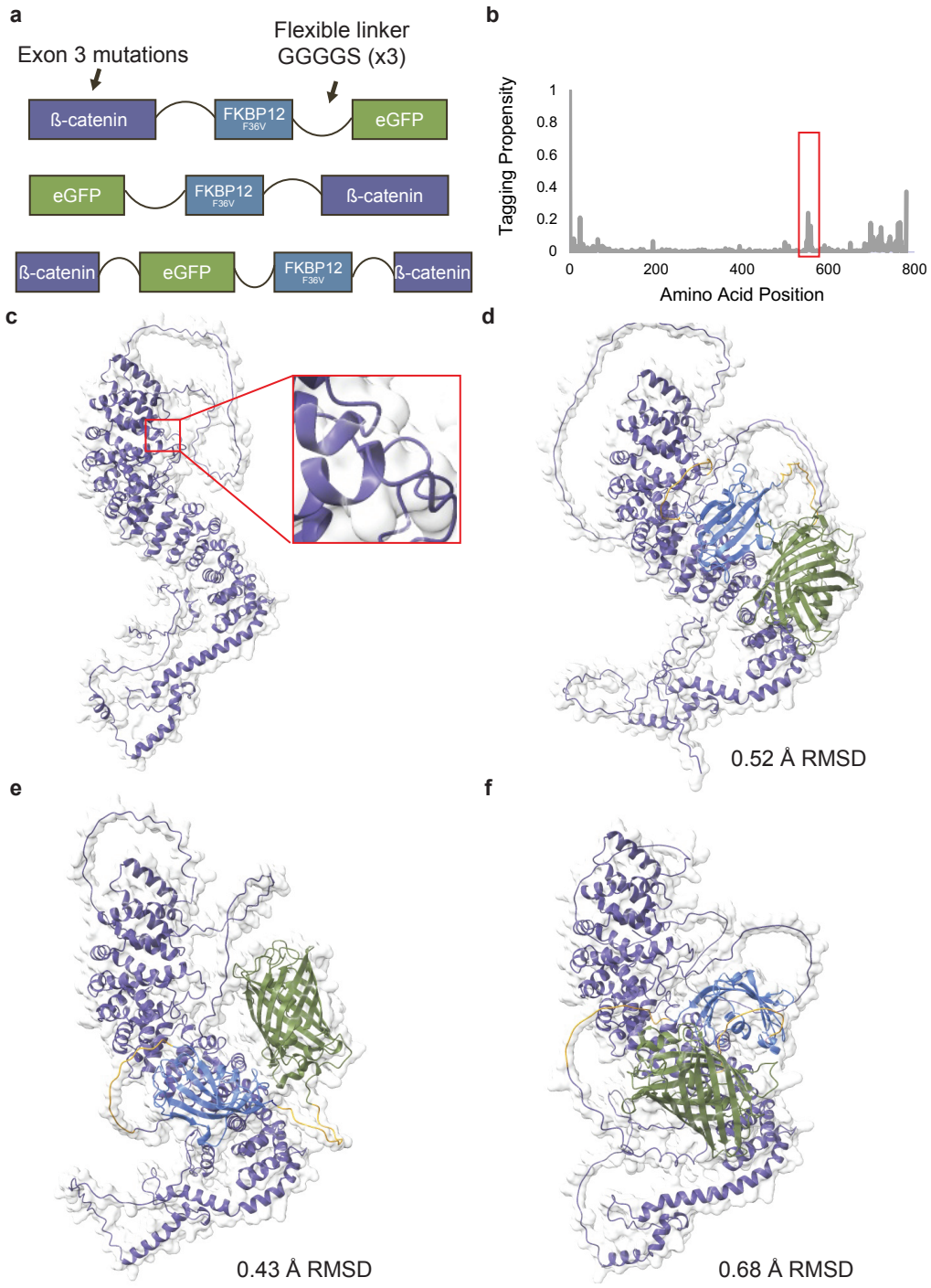

Figure 4 Tagging positions in β-catenin **a)** Schematic representation of 3 constructs designed containing β-catenin, FKBP12^{F36V} and GFP connected by GGGGS (x3) flexible linker. The first construct was fused at the C-terminus, the second at the N-terminus, and the third was internally fused, then exon 3 mutations (e.g., S33F, T41A & S45F) were added to each of the construct. **b)** Dr Joe Mash's computational tool predicted 'tolerable' sites for tagging β-catenin, the highlighted peak indicates the internal site used for fusion. **c)** 3D protein model of wild-type β-catenin generated using AlphaFold2 and displayed with ChimeraX. The highlighted region in the model represents the internal fusion site. **d-f)** 3D models were generated using AlphaFold2 and displayed with ChimeraX. RMSD score obtained when superimposed with wild-type β-catenin (c) using ChimeraX. **d)** 3D protein model of internally fused β-catenin. **e)** 3D protein model of C-terminally fused β-catenin. **f)** 3D protein model of N-terminally fused β-catenin.

To assess the degradation efficiency cells were treated with PROTACs that recruit $Cul2^{VHL}$ ($dTAG^{V}$-1) or $CUL4A^{CRBN}$ (dTAG-13) to the β-catenin $FKBP12^{F36V}$ fusions for 2 hours and monitored via flow cytometry. In HeLa cell lines, $dTAG^{V}$-1 degraded C-terminal and internal fusions with a degradation maximum (D_{max}) of 91% and 94%, respectively (Figure 6a). dTAG-13 degraded these constructs relatively modestly, with a D_{max} of 57% and 31%, respectively. Strikingly, N-terminal fusions only reached D_{max} of 4% with $dTAG^{V}$-1 and 1% with dTAG-13. In addition, the difference in the DC_{50} between constructs was observed. C-terminal and internal fusions that were treated with $dTAG^{V}$-1 had DC_{50} of 17nM and 42nM, respectively. In contrast, DC_{50} with dTAG-13 was achieved with 45nM and 51 nM (Figure 6a). Thus, the potency of $dTAG^{V}$-1 showed a moderate dependency on tag position, whereas the potency of dTAG-13, which was a less effective degrader of both constructs, did not. A similar pattern of D_{max} was seen in HEK293 cell lines. $dTAG^{V}$-1 induced degradation of C-terminal and internal fusions with D_{max} values of 69% and 77%, respectively (Figure 6b). Meanwhile, dTAG-13 showed less efficient degradation with D_{max} values of 63% and 44%. Similar to HeLa cells, N-terminal fusion showed a low D_{max}, reaching only 19% with $dTAG^{V}$-1 and 17% with dTAG-13. Although the N-terminal fusion remained poorly degraded in HEK293 cells, there was a substantial increase in degradation relative to HeLa. Overall, the extent of degradation (D_{max}) in HEK293 cells tended to be lower than in HeLa cells at this 2-hour timepoint. DC_{50} in HEK293 cells was more variable, C-terminal fusion reached only 30nM, while internal fusion was 103nM with $dTAG^{V}$-1. DC_{50} with dTAG-13 was achieved at 12nM and 47nM for C-terminal and internal fusion, respectively (Figure 6b). Thus, the potency of $dTAG^{V}$-1 and dTAG-13 showed a high dependency on tag position. Future experiments could test the expression of

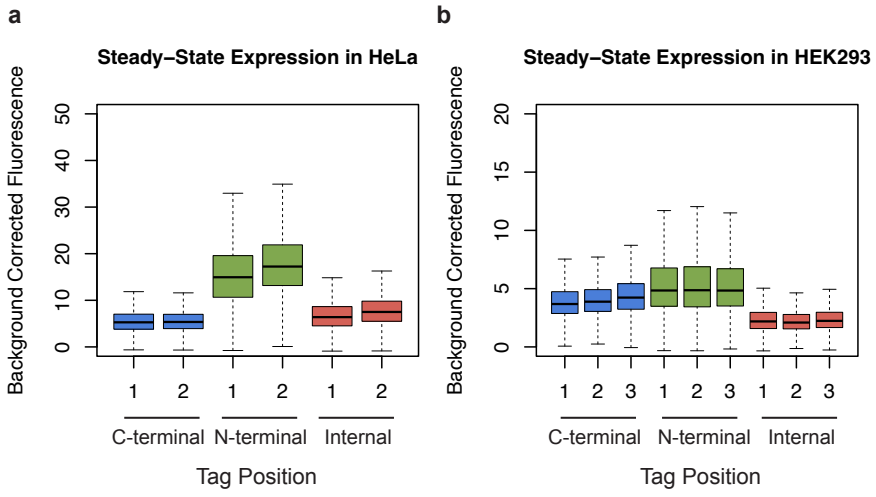

Figure 5 Steady-state comparison in tagged β-catenin at different positions and cell lines. **a)** The boxplots show steady-state expression of fused β-catenin in HeLa cells, presented as background corrected fluorescence normalised to 100. The box represents the interquartile range (IQR), with the median depicted as a central line within the box. Whiskers extend to the minimum and maximum values within 1.5 times the IQR. The analysis is based on a minimum of 10,000 cells using FlowJo. Two replicates (displayed as 1 and 2) were conducted on different days, utilising cells from the same initial population. **b)** The boxplots show steady-state expression of fused β-catenin in HEK293 cells, presented as background corrected fluorescence normalised to 100. The box parameters as described above. The analysis is based on a minimum of 10,000 cells using FlowJo. Three replicates (displayed as 1, 2 and 3) were conducted on different days, utilising cells from the same initial population.

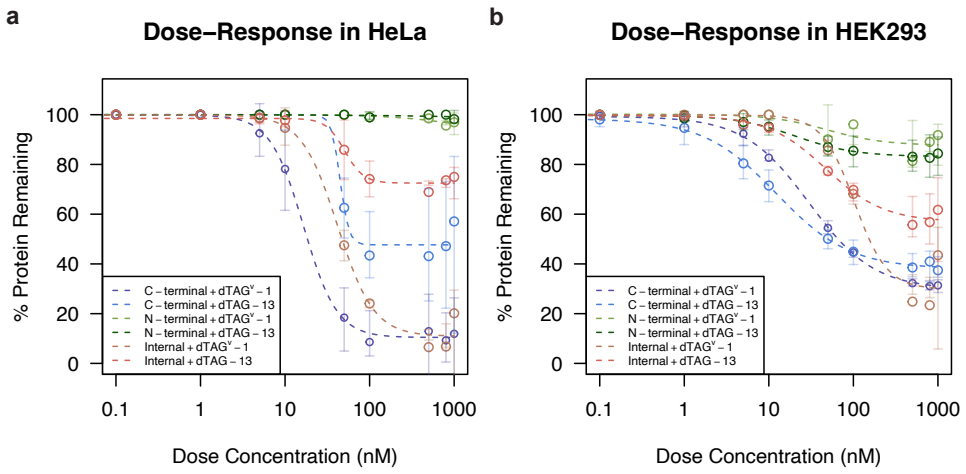

ß-catenin Constructs in HeLa	DC_{50} (nM)	D_{max} (%)
C-terminal + dTAG^V-1	16.6	91.4
C-terminal + dTAG-13	44.7	56.9
N-terminal + dTAG^V-1	1311	4.39
N-terminal + dTAG-13	-	1.78
Internal + dTAG^V-1	41.7	93.5
Internal+ dTAG-13	50.7	31.1

ß-catenin Constructs in HEK293	DC_{50} (nM)	D_{max} (%)
C-terminal + dTAG^V-1	29.9	68.9
C-terminal + dTAG-13	12.3	62.5
N-terminal + dTAG^V-1	48.9	18.6
N-terminal + dTAG-13	20.3	17.4
Internal + dTAG^V-1	103	76.6
Internal+ dTAG-13	47.1	44.3

Figure 6 Degradability comparison in tagged β-catenin at different positions and cell lines. **a)** The dose-response graph displays normalised background corrected fluorescence unit, set at 100%. The table presents half-maximal degradation concentration (DC_{50}) and degradation maximum (D_{max}) calculations following a 2 h incubation with dTAG^V-1 or dTAG-13 in HeLa cell lines. The mean of two replicates was obtained from FlowJo 10 analysis and used for DC_{50} and D_{max} calculations. The error bars represent the standard deviation in the graph generated in R. Replicates were conducted on different days, utilising cells from the same initial population. **b)** The dose-response graph displays normalised background corrected fluorescence unit, set at 100%. The table presents DC_{50} and D_{max} calculations following a 2 h incubation with dTAG^V-1 or dTAG-13 in HEK293 cell lines. Following the same protocol as above.

relevant E3 ligase subunits and/or determine whether the same pattern holds true at later time points.

4.2. Investigating Poor Degradation of N-terminal Fusion

To explain the poor degradation of N-terminal fusion proteins, I hypothesised that the GFP reporter module could become detached from the degron following linker hydrolysis, meaning that GFP no longer accurately reported on the degradation of β-catenin. Consistent with this, western blots revealed the presence of a ~30 kDa band specific to cells expressing the N-terminal fusion, which was detected by an anti-GFP antibody in the HeLa cell line (Figure 7a), which was also observed in the HEK293 cell line expressing the same fusion construct (Figure 7b). These findings suggest that, specifically in the context of the N-terminal fusion, GFP undergoes proteolytic separation from FKBP12^{F36V}:β-catenin. This elucidates the absence or partial GFP degradation in this particular cell line. As FKBP12^{F36V} has a molecular weight of only 12 kDa, distinguishing whether the linker between FKBP12^{F36V} and β-catenin remained intact and if a ternary complex is formed with E3 ligase proved challenging.

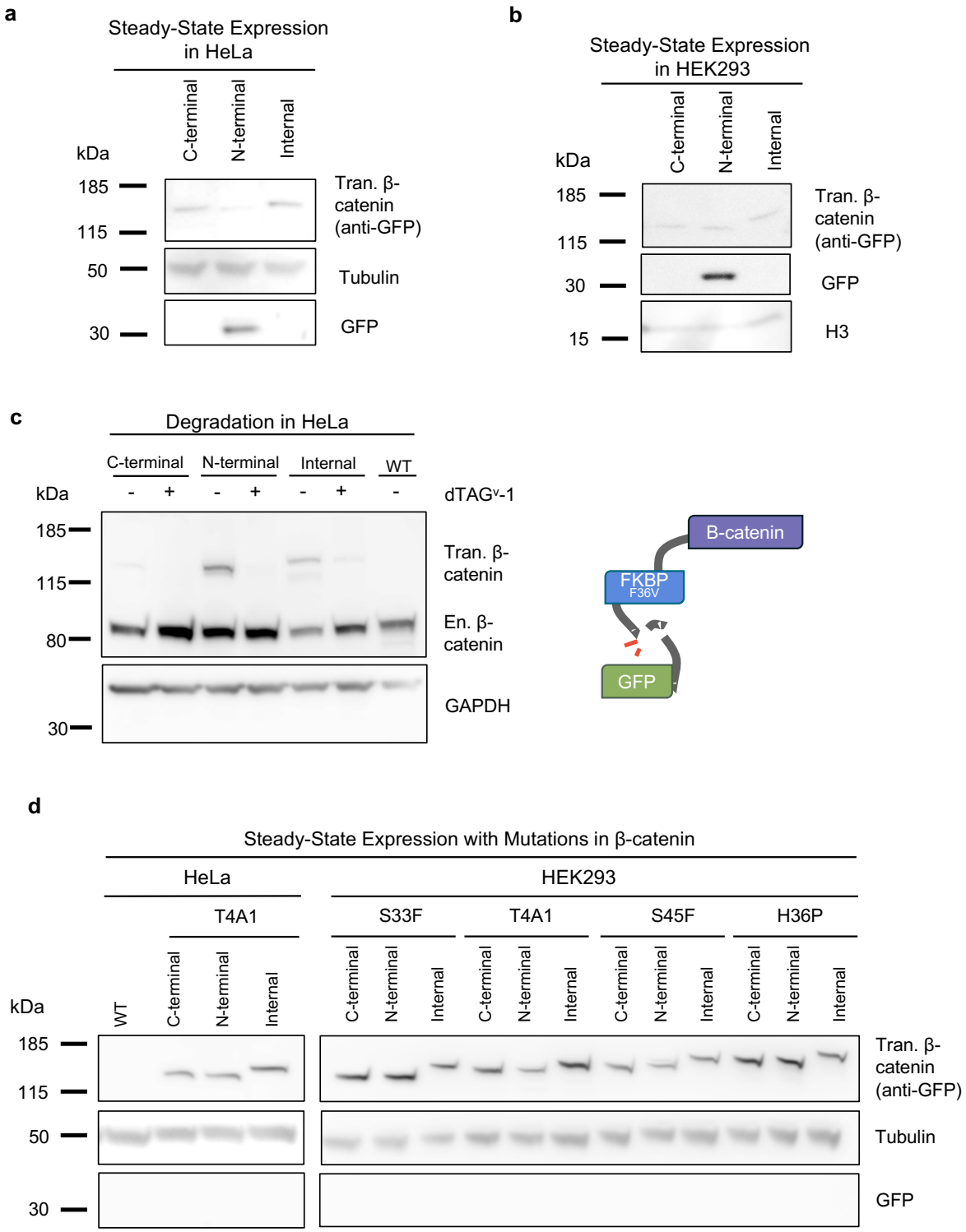

Figure 7 N-terminus fusion undergoes proteolytic separation. **a)** Western blot of steady-state expression of fused β-catenin was probed with antibody against GFP. Band at ~30 kDa indicating GFP proteolytic separation in HeLa cell lines. **b)** Western blot of steady-state expression of fused β-catenin was probed with antibody against GFP. Band at ~30 kDa indicating GFP proteolytic separation in HEK293 cell lines. **c)** Fused β-catenin degradation with $dTAG^{V}$-1 for 2h at 200nM in HeLa cell lines showed N-terminal degradation, indicating only GFP proteolytic separation. Schematic representation of linker breakage between GFP and $FKBP12^{F36V}$ tag. **d)** Western blot of steady-state expression of fused β-catenin with native degron mutations were probed in HeLa and HEK293 cells with antibody against GFP. No band at ~30 kDa was observed. Tran-transgene β-catenin, En-endogenous β-catenin.

To address this, degradation induced by dTAG^{V}-1 was analysed through a western blot, which showed degradation of β-catenin and therefore provided evidence that the linker separating β-catenin and FKBP12^{F36V} remained intact (Figure 7c). Surprisingly, the introduction of oncogenic mutations into the native degron of tagged β-catenin prevented hydrolysis in both HeLa and HEK293 cells (Figure 7d), mutations further discussed in the following section. For the remaining experiments, I therefore focused on internal and C-terminal fusions.

4.3. Evaluating Stabilising Mutations of Different Effect Sizes on Steady-State Expression and Degradation Kinetics

To better understand the impact of stabilising mutations that disrupt natural turnover pathways on the kinetics of TPD, three distinct missense mutations were introduced within the native degron into constructs containing a C-terminal tag in HEK293 cells, which are commonly used in research about the Wnt pathway. The quantification of

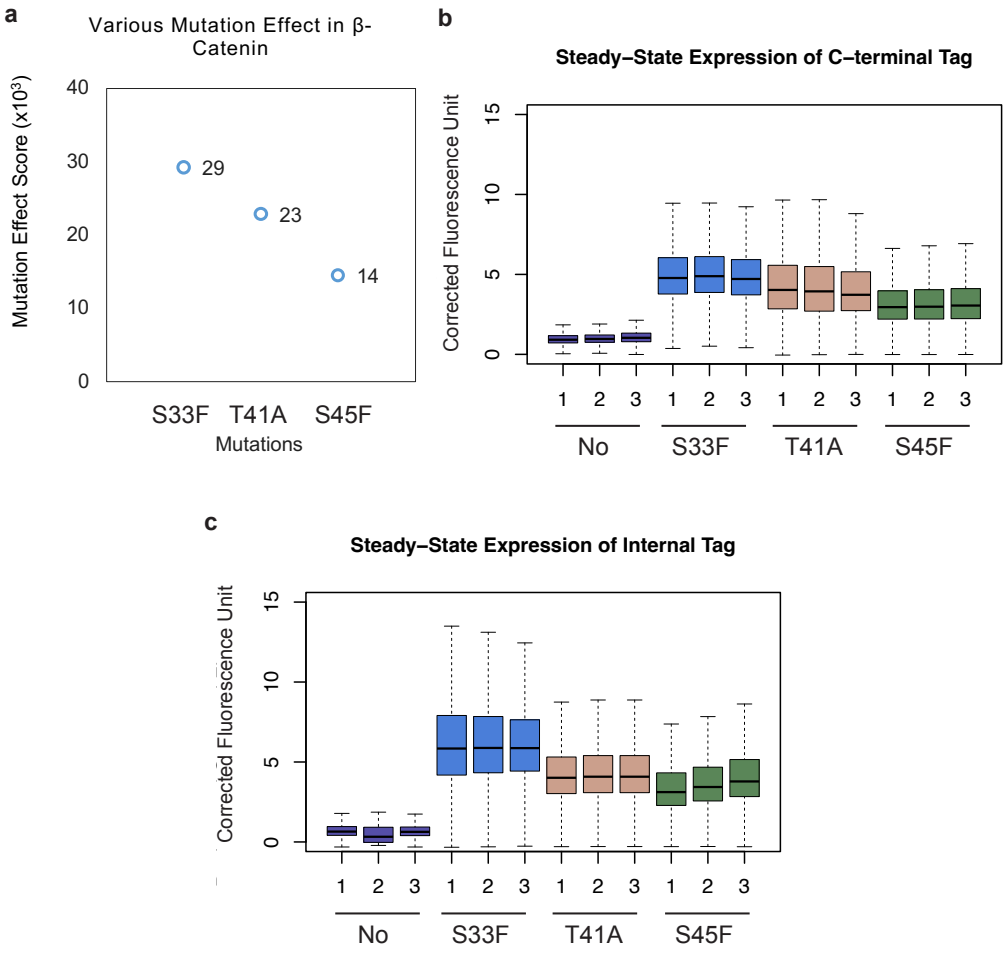

Figure 8 Steady-state comparison in C-terminally and internally tagged β-catenin between missense mutations in native degron in HEK293 cell line. **a)** The graph shows various mutation effects in β-catenin's native degron. The mutation effect score was taken from Krishna et al., 2023. **b)** The boxplots show steady-state expression of C-terminally fused β-catenin with native degron mutations. **c)** The boxplots show steady-state expression of internally fused β-catenin with native degron mutations. **b-c)** The steady state presented as background corrected fluorescence normalised to 100. The box parameters as described in Figure 5. The analysis is based on a minimum of 10,000 cells using FlowJo. Three replicates (displayed as 1, 2 and 3) were conducted on different days, utilising cells from the same initial population.

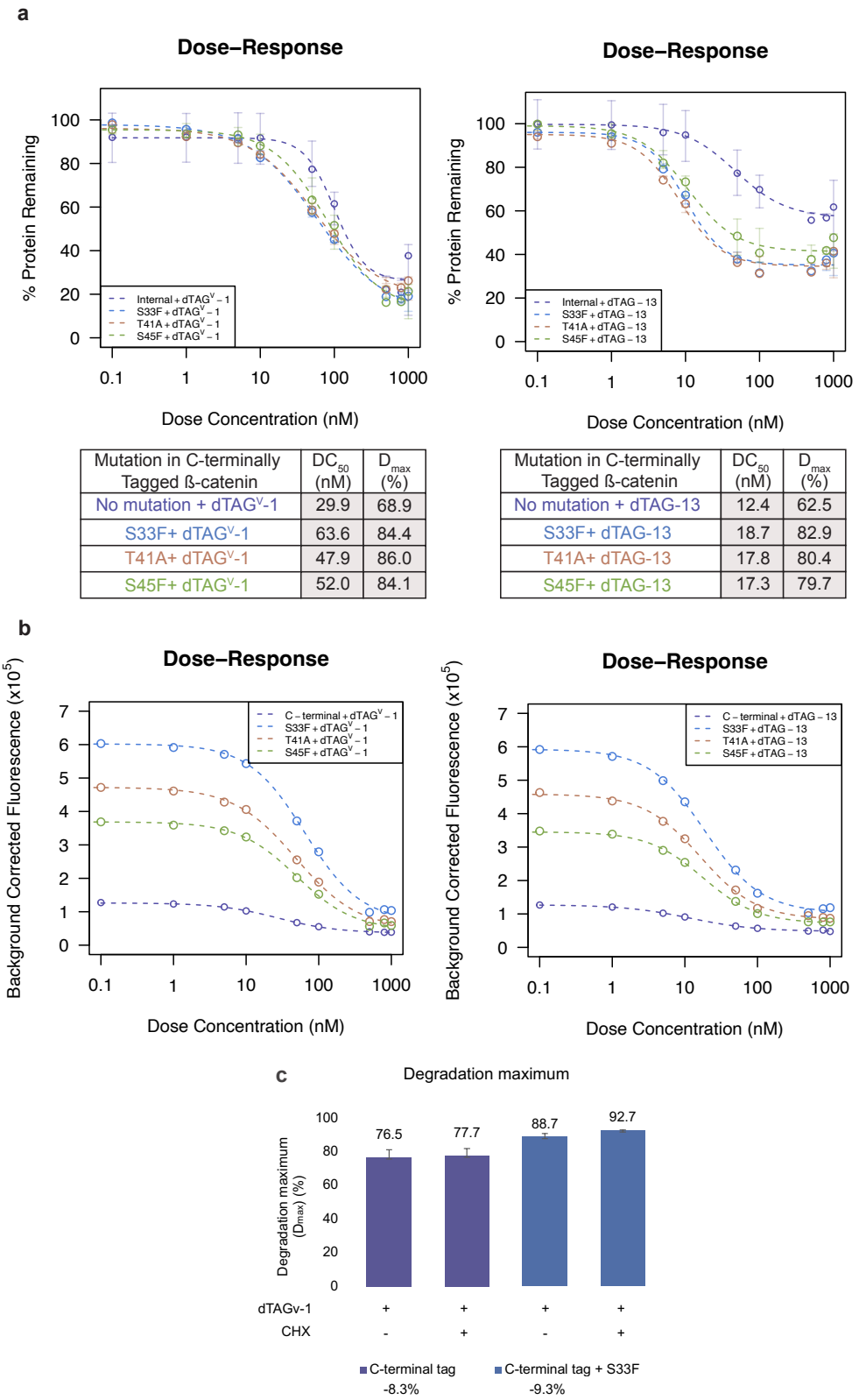

Mutation in C-terminally Tagged ß-catenin	DC_{50} (nM)	D_{max} (%)
No mutation + dTAG^V-1	29.9	68.9
S33F+ dTAG^V-1	63.6	84.4
T41A+ dTAG^V-1	47.9	86.0
S45F+ dTAG^V-1	52.0	84.1

Mutation in C-terminally Tagged ß-catenin	DC_{50} (nM)	D_{max} (%)
No mutation + dTAG-13	12.4	62.5
S33F+ dTAG-13	18.7	82.9
T41A+ dTAG-13	17.8	80.4
S45F+ dTAG-13	17.3	79.7

Figure 9 Degradation kinetics comparison in C-terminally tagged β-catenin between missense mutations in native degron in HEK293 cell line. **a)** The dose-response graph displays normalised background corrected fluorescence unit, set at 100%. The table presents half-maximal degradation concentration (DC_{50}) and degradation maximum (D_{max}) calculations following a 2 h incubation with dTAG^V-1 or dTAG-13. The mean of two replicates was obtained from FlowJo 10 analysis and used for DC_{50} and D_{max} calculations. The error bars represent the standard deviation in the graph generated in R. Replicates were conducted on different days, utilising cells from the same initial population. **b)** The dose-response graph displays background corrected fluorescence unit from the same dataset as above. **c)** The degradation maximum graph shows changes in D_{max} with and without cycloheximide. (-) shows untreated cells, while (+) shows CHX or/and dTAG^V-1 treated cells for 2 h. Two replicates were conducted on different days, utilising cells from the same initial population. The error bars represent the standard deviation of those two replicates.

GFP:dTAG - fused β-catenin via flow cytometry showed higher levels of fluorescence in cells with missense mutations in native degron than no mutation fusion. A previous study calculated Mutation Effect Scores (MES) for all *CTNNB1* native degron missense substitutions and identified S33F as a high effect, T41A as moderate and S45F as a low effect mutation (Figure 8a) (Krishna *et al.*, 2023). At the steady state, the mutation effect size had the equivalent effect on the tagged β-catenin stability in both C-terminal and internal fusions; S33F showed the highest level of expression, T41A moderate and S45F low (Figure 8b-c).

To assess how stabilising oncogenic mutations in a native degron affected the PROTAC-mediated degradation kinetics of tagged proteins, cells were treated with

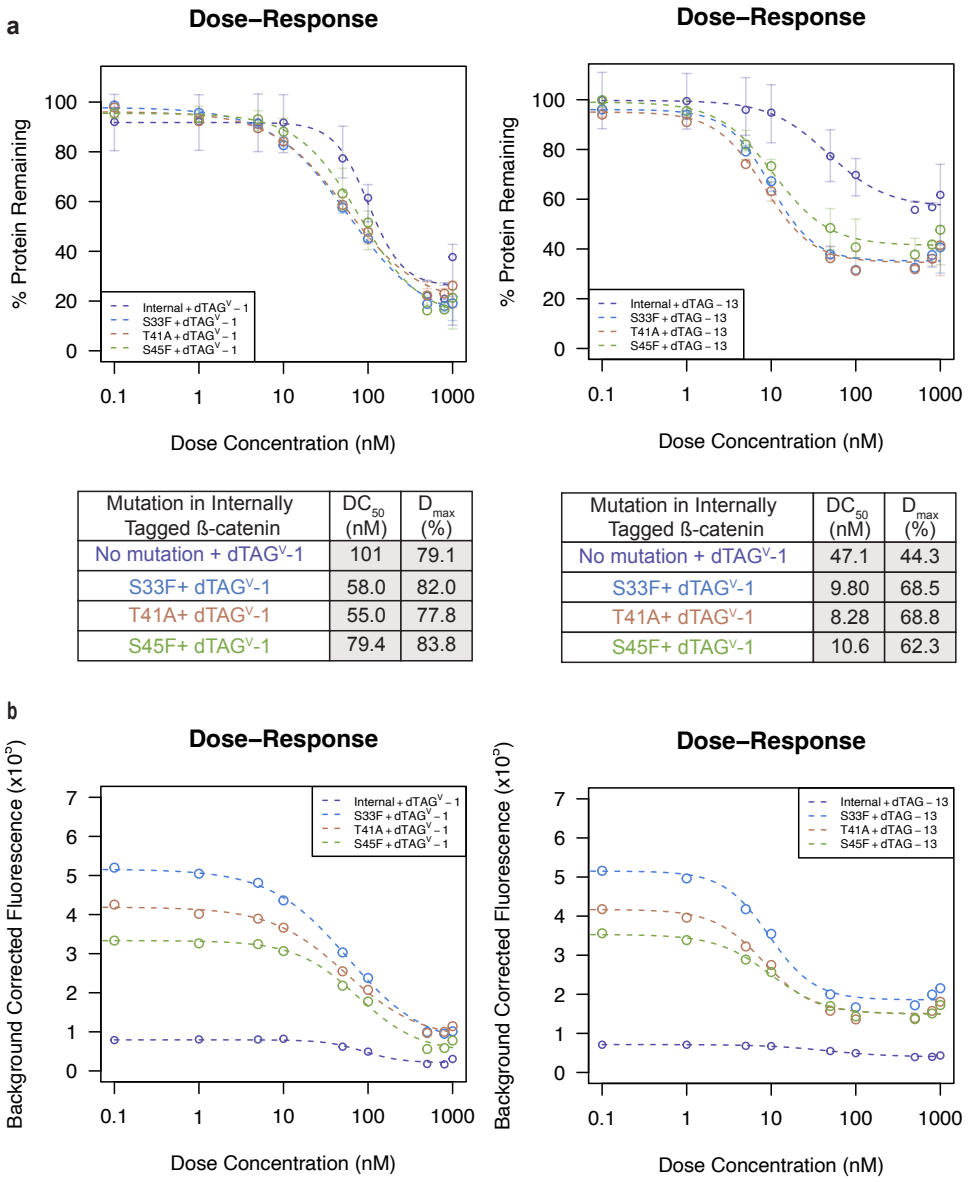

Mutation in Internally Tagged ß-catenin	DC_{50} (nM)	D_{max} (%)
No mutation + dTAG^V-1	101	79.1
S33F+ dTAG^V-1	58.0	82.0
T41A+ dTAG^V-1	55.0	77.8
S45F+ dTAG^V-1	79.4	83.8

Mutation in Internally Tagged ß-catenin	DC_{50} (nM)	D_{max} (%)
No mutation + dTAG^V-1	47.1	44.3
S33F+ dTAG^V-1	9.80	68.5
T41A+ dTAG^V-1	8.28	68.8
S45F+ dTAG^V-1	10.6	62.3

Figure 10 Degradation kinetics comparison in internally tagged β-catenin between missense mutations in native degron in HEK293 cell line. **a)** The dose-response graph displays normalised background corrected fluorescence unit, set at 100%. The table presents half-maximal degradation concentration (DC_{50}) and degradation maximum (D_{max}) calculations following a 2 h incubation with dTAG^V-1 or dTAG-13. The mean of two replicates was obtained from FlowJo 10 analysis and used for DC50 and Dmax calculations. The error bars represent the standard deviation in the graph generated in R. Replicates were conducted on different days, utilising cells from the same initial population. **b)** The dose-response graph displays background corrected fluorescence unit from the same dataset as above.

dTAG^V-1 and dTAG-13 and protein degradation was monitored by flow cytometry. In HEK293 cell lines with C-terminal fusion, D_{max} increased from 69% to 84-86% in stabilised β-catenin with dTAG^V-1, indicating a larger fraction of the mutant protein pool was degraded compared to wildtype. Consistently, dTAG-13 increased from 63% to 70-86% (Figure 9a). However, to achieve DC_{50} with dTAG^V-1, concentrations ranging from 48-64 nM were required, representing an increase from 30 nM observed in the no mutations scenario, dTAG-13 increase was slight by only ~ 5 nM (Figure 9a). Thus, dTAG-13 had a greater potency in stabilised β-catenin than dTAG^V-1.

Internal fusion with dTAG^V-1 showed a decrease in DC_{50} from 101 nM to 58-79 nM in stabilised β-catenin, while dTAG-13 ranged from 8-11 nM, indicating a decrease from the 47nM observed in the absence of mutations (Figure 10a).

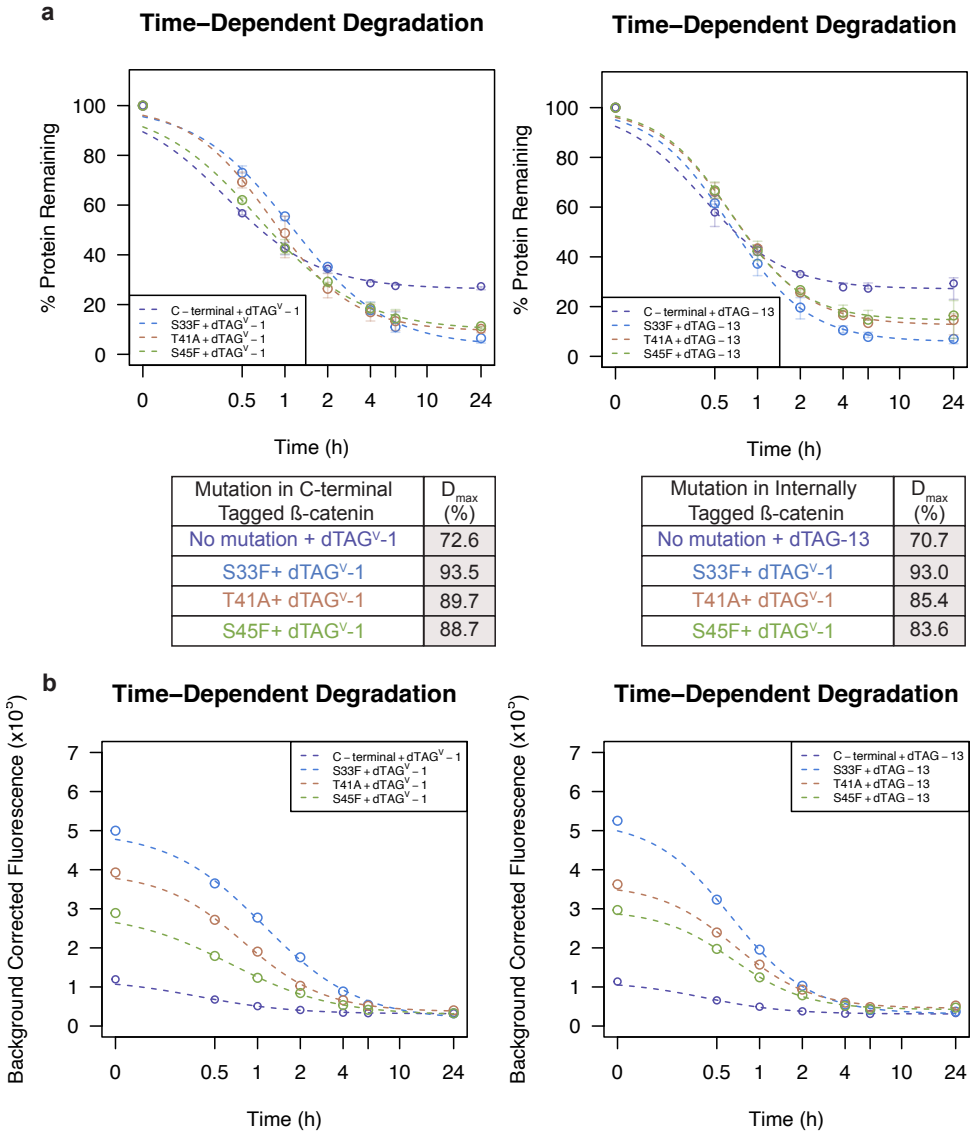

Mutation in C-terminal Tagged ß-catenin	D_{max} (%)
No mutation + dTAG^V-1	72.6
S33F+ dTAG^V-1	93.5
T41A+ dTAG^V-1	89.7
S45F+ dTAG^V-1	88.7

Mutation in Internally Tagged ß-catenin	D_{max} (%)
No mutation + dTAG-13	70.7
S33F+ dTAG^V-1	93.0
T41A+ dTAG^V-1	85.4
S45F+ dTAG^V-1	83.6

Figure 11 Time-dependant degradation in C-terminally fused β-catenin with missense mutations in native degron in HEK293 cell line. **a)** The time-dependent degradation graph displays normalised background corrected fluorescence unit, set at 100%. The table presents degradation maximum (D_{max}) calculations following a 0 - 24 h incubation with dTAG^V-1 or dTAG-13. The mean of two replicates was obtained from FlowJo 10 analysis and used for D_{max} calculations. The error bars represent the standard deviation in the graph generated in R. Replicates were conducted on different days, utilising cells from the same initial population. **b)** The time-dependent degradation graph displays background corrected fluorescence unit from the same dataset as above.

Relocating the tag to the internal position caused a notable increase in PROTAC potency, characterised by a lower DC_{50} but higher D_{max} (Figure 10a). Conversely, the C-terminal tag, at the same timepoint, exhibits a higher maximum degradation and higher DC_{50}. This data supported the idea that a higher amount of PROTACs was required to degrade an equivalent fraction of target protein when the initial abundance was higher.

Normalising protein to a percentage facilitates a standardised comparison of degradation kinetics despite the difference in initial expression level. In contrast, choosing the less conventional method of plotting fluorescence values provides a direct insight into the absolute magnitude of changes in GFP expression. Therefore, when fluorescence values after degradation were compared, they revealed that the C-

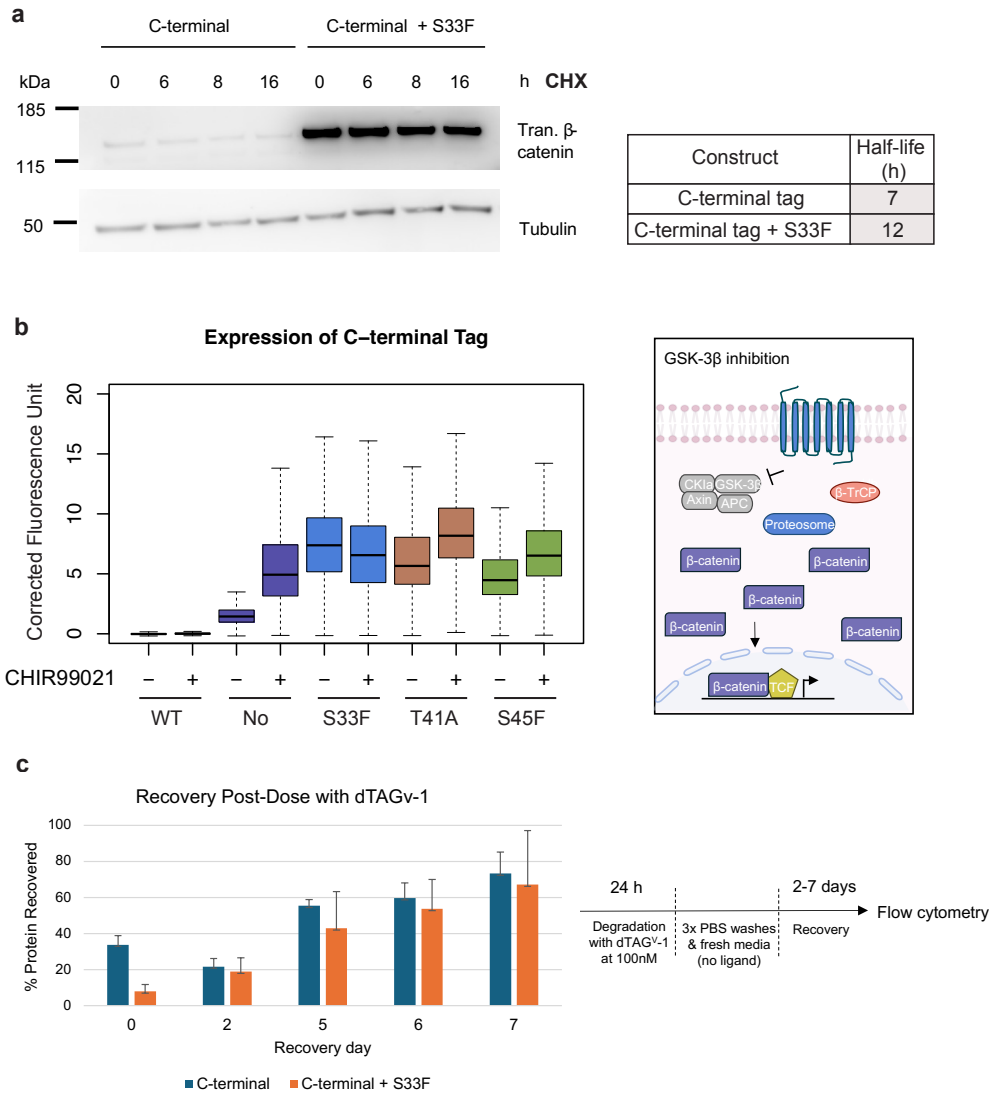

Construct	Half-life (h)
C-terminal tag	7
C-terminal tag + S33F	12

Figure 12 Turnover of C-terminally tagged β-catenin **a)** Western blot of expression of fused β-catenin after cycloheximide chase assay (100µg/mL) was probed with antibody against CTNNB1, represented as a band at ~130 kDa. The table shows the calculated half-life based on 2 replicates conducted on different days, utilising cells from the same initial population. **b)** The boxplots show expression of C-terminally fused β-catenin with native degron mutations, presented as background corrected fluorescence, normalised to 100. (-) shows untreated cells, while (+) shows CHIR99021 (10nM for 24 h) treated cells. The box parameters as described in Figure 5. The analysis is based on a minimum of 10,000 cells using FlowJo of two replicates mean. The replicates were conducted on different days, utilising cells from the same initial population. Schematic representation of GSK3β inhibition by CHIR99021. **c)** The graph shows the recovery after $dTAG^V$-1 degradation. Two replicates were conducted on different days, utilising cells from the same initial population. The error bars represent the standard deviation of those two replicates. Schematic representation of the timeline of this experiment.

terminal fusion with a stabilising mutation, despite having higher expression levels than the fusion without mutation, reached nearly the same absolute protein level after degradation with dTAG^{V}-1, while this effect was less pronounced with dTAG-13 (Figure 9b). Additionally, the internal fusion exhibited an even lower absolute protein level after degradation with dTAG^{V}-1 and to an even lesser extent with dTAG-13 (Figure 10b). At the highest concentration in both fusions, there is a potential indication of the hook effect. To explore whether longer exposure can lead to higher D_{max}, C-terminally tagged cells were treated for the time course of 24 h. Constructs without mutations achieved 71-73% of D_{max} with dTAG^{V}-1 and dTAG-13, respectively. While stabilising mutation reached D_{max} of 93-84% (Figure 11a). Longer exposure with ligands led to higher D_{max} but not complete degradation. Additionally, despite varying stabilization effects, all constructs reached nearly the same absolute level of tagged β-catenin (Figure 11b). This suggests that changes in stability do not substantially affect the absolute level of protein remaining after TPD.

I next considered factors other than baseline stability that might affect the absolute D_{max} value. To understand whether the rate of production affected PROTAC-mediated degradation, protein production was inhibited using cycloheximide, and the maximum degradation was investigated. After incubation for 2 h with dTAG^{V}-1 for degradation and CHX for inhibition of protein production, it was found that C-terminally tagged β-catenin showed a slight increase of 1% in D_{max}, while stabilised S33F variant exhibited increase of 4% (Figure 9c). A decrease in the absolute level of tag protein was observed to be between 8-9%. Although more experimental replicates would be required to confidently measure changes on this scale, the data are consistent with the idea that degradation maximum can be influenced by the protein production.

4.4. Determining Tagged β-Catenin Turnover

Confirming the stabilizing effect of the S33F mutation in a tagged β-catenin variant was important for understanding protein abundance regulation. Although S33F is known to enhance β-catenin stability, it is unclear whether this effect extends to the tagged variant. Cycloheximide chase assay revealed a notably extended half-life of 12 h with S33F mutation, whereas the wild type displayed a shorter half-life of 7 h. This observation suggested that the introduction of mutation indeed enhances protein stability, resulting in a prolonged presence of the mutant β-catenin variant within the cellular environment (Figure 12a).

To assess whether tagged β-catenin was undergoing turnover via SCF$^{\beta TrCP}$-mediated degradation, I looked at the steady-state expression when GSK3β was inhibited. This should prevent the formation of the destruction complex, resulting in the accumulation of tagged β-catenin. Cell lines with no mutation, as well as those with moderate T41A and low S45F mutation effect, showed a substantial increase in stability. Hence, showing the native degron functionality through normal β-catenin turnover, while S33F was not further stabilised. S33F was previously determined to be a high-effect mutation (Krishna et al 2023, Figure 12b) possibly explaining why destruction complex inhibition had no additional effect on native degron function.

To determine the recovery rate following dTAG^{V}-1-mediated degradation, cells were monitored over several days. It was found that both C-terminally tagged β-catenin and the S33F variant exhibited slow recovery following PROTAC washout, reaching approximately 50% by days 5 and 6, and approximately 70% by day 7 (Figure 12c).

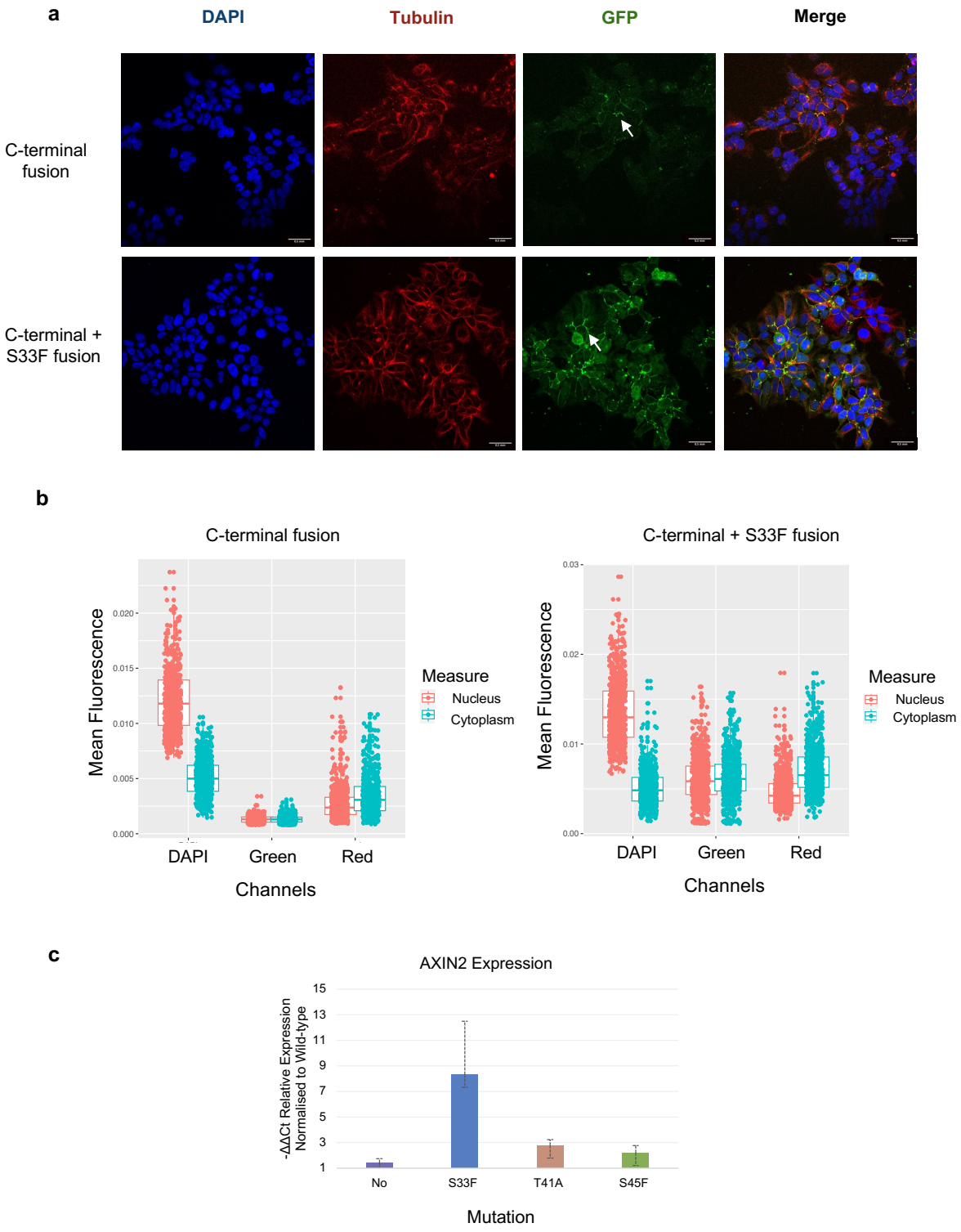

Figure 13 Function of C-terminally tagged β-catenin **a)** Fluorescence images of C-terminally fused β-catenin with and without S33F mutation, arrows pointing to adherence junctions. DAPI staining in blue represents the nucleus, red fluorescence corresponds to tubulin, and green fluorescence indicates GFP-tagged β-catenin. **b)** The boxplots show mean fluorescence in different channels, showing individual cell mean fluorescence unit. The nucleus and cytoplasm fluorescence were calculated with CellProfiler using a minimum of 100 cells. **c)** The bar plot shows -ΔΔCt relative AXIN 2 expression normalised to wild-type. Three replicates were conducted on different days, utilising cells from the same initial population. The error bars represent the standard deviation of those three replicates.

4.5. Determining Transcriptional Function of Tagged β-Catenin

Previously it was demonstrated that β-catenin with C-terminal fluorescent protein fusions can still regulate Wnt target genes (Ambrosi *et al.*, 2022). To investigate whether my β-catenin construct, which was also C-terminally tagged, β-catenin retained the ability to regulate target genes, I used HEK293 cells, which are often used to investigate the Wnt pathway in the literature. Immunofluorescence of boosted GFP showed normal C-terminally fused β-catenin localisation at the cell membrane region, likely representing adherens junctions (Figure 13a). Tagged β-catenin also showed the expected accumulation in the cytoplasm as well as in nucleus in response to the S33F native degron mutation (Figure 13b). To see whether tagged β-catenin accumulation in the nucleus resulted in increase of Wnt target gene transcription, analysis by qPCR was performed, which showed an 1.4-fold increase in Axin 2 in response to tagged β-catenin, while stabilisation with high effect S33F mutation resulted in 8-fold increase, 3-fold increase was observed with moderate effect T41A mutations and 2-fold increase with low effect S45F mutation (Figure 13c). This suggested that tagged β-catenin retains its transcriptional function, and mutations in the native degron had the expected effect on the level of target gene activation.

5. DISCUSSION

Oncogenic transcription factors such as β-catenin are difficult to modulate using small molecules (Uitdehaag *et al.*, 2015), but TPD strategies provide new avenues to explore previously undruggable proteins (Samarasinghe and Crews, 2021), with some covalent degraders successfully achieving transcription factor degradation (Gowans *et al.*, 2024), making this a highly promising field of research. In this study, I used degron tagging rather than direct targeting of β-catenin. Although degron tagging is not a direct therapeutic strategy, it provides the means to understand variables which could govern the success of TPD, such as how oncogenic mutations, specifically those which act by stabilising a target protein, influence degradation kinetics, which is not explicitly addressed in the literature. I investigated how synthetic degrons fused at different positions of β-catenin affect its expression and turnover, and what effect protein stability had on PROTAC degradation kinetics. My main findings were that the position of the synthetic degron affected both the steady-state expression and degradation kinetics of tagged β-catenin. The fusion at the C-terminus did not substantially disrupt the native degron and it retained the transcriptional functions of β-catenin, indicating that these modifications do not interfere with the protein's essential roles in cellular processes. Additionally, I found that while the stability of β-catenin influenced by exon 3 mutations did not affect the maximum degradation (Figure 9b), the rate of β-catenin production did (Figure 9c). Given that β-catenin is activated in human cancer almost exclusively via mechanisms that enhance stability, this information is of limited direct relevance to clinical strategies for targeting this protein. However, for other oncogenic targets where activation can occur via either stabilisation or enhanced production (e.g. via copy number amplification) (Pessoa *et al.*, 2022), my results suggest that the activation mechanism could influence the efficacy of targeted protein degradation.

The developed model system facilitated the study of β-catenin degradation by fusing synthetic degrons at various positions. Strategies like dTAG require protein tagging, and factors such as the specific degron tag, construct design, and the target

itself heavily influence expression and degradability (Bondeson *et al.*, 2022). Incorporating a fusion tag containing GFP and the synthetic degron tag FKBP12^{F36V}, facilitated convenient analysis by flow cytometry. GFP is commonly used in such fusions to estimate protein location and quantity (March, Rao and Bentley, 2003). Although the fusion tag may potentially interfere with normal protein function and turnover, which occurrence is not uncommon in the literature, this does not necessarily prevent the acquisition of relevant information.

All constructs were transfected using the Flp-in system to establish stable cell lines. The Flp-In system offered distinct advantages in this context, facilitating the integration of different transgene variants into the same safe harbour within a specific genomic locus via Flp/FRT recombinase, where the transgenes are typically present as single copies. This reduces the potential for gene silencing or overexpression artefacts associated with multiple copies, which are common in random integration (Szczesny *et al.*, 2018). Since the promoter and the locus of genomic integration are the same for all constructed cell lines, this allowed consistent expression and comparability across all constructed cell lines. Additionally, the introduction of the transgene instead of tagging the endogenous protein enabled the investigation of how mutations affected expression and degradability, without affecting the function of the endogenous protein or causing unintended effects on cellular physiology in the absence of the protein being degraded. Therefore, this model allowed a direct comparison of the effects of the tag site on expression and degradation, as well as the impact of stabilising mutations.

The effect of synthetic degron tag position on β-catenin degradation kinetics and expression suggested that precise engineering of degron tags is essential for optimising TPD strategies. The N-terminal fusion showed the highest steady-state expression, yet poor degradation was observed (Figure 5 and 6), due to proteolytic separation of GFP (Figure 7a-b) caused by linker cleavage. The GGGGS (x3) linker used serves as a flexible linker, providing spatial separation between domains to minimise steric interference and enhance stability, folding, and overall biological activity (Chen, Zaro and Shen, 2013). Notably, the same linker was present on either side of the tag, however despite GFP proteolysis the synthetic tag remained fused and functioning (Figure 7c). Interestingly, when mutations were introduced into the native degron, hydrolysis of GFP was not observed in both HeLa and HEK293 cells (Figure 7d), this could indicate that separation was influenced by normal turnover of β-catenin by SCF$^{\beta TrCP}$ because the native degron mutation could reduce or prevent SCF$^{\beta TrCP}$ initiated degradation. Further experiments are needed to confirm this hypothesis and ongoing linker-related investigations by a PhD student in the Wood lab aims to provide additional insights.

Both C-terminal and internal fusions demonstrated comparable expression levels, with slight variations among cell lines (Figure 5). A higher D_{max} was achieved in HeLa cell lines treated with dTAG^{V}-1, than HEK293 (Figure 6). Additionally, HeLa cell lines had a substantial decrease in degradation efficacy with dTAG-13 while HEK293 cell lines showed less variation between both ligands. The literature lacks a direct examination of VHL and CRBN E3 ligase expression in HeLa and HEK293 cells. However, due to the different origins of the cell lines, heterogeneity in E3 ligase is expected (Kramer and Zhang, 2022). Across cell lines, constructs, and native degron mutations, dTAG-13 consistently showed lower D_{max} values, possibly indicating certain E3 ligases' superior efficiency in degrading this specific protein (Békés et al., 2022).

Previous studies used fluorescently tagged β-catenin to analyse its kinetics and dynamics, which also looked at the wild-type and mutant β-catenin (Jamieson, Sharma and Henderson, 2011; Kafri et al., 2016; Ambrosi et al., 2022). By contrast, here the study focused on the impact of β-catenin stability on degradation kinetics. It seems reasonable to infer that a lower DC_{50} (i.e., more potent degradation) indicates more efficient formation of functional ternary complexes. In this study, the DC_{50} was observed to be lower in no mutation C-terminal fusion compared to no mutation internal fusion. However, introduced mutations had the effect on DC_{50}, which was consistent across tag positions: the DC_{50} increased with a C-terminal fusion, while it decreased with an internal fusion. The more potent degradation was observed with dTAG-13 ligand than TAG^{V}-1. Thus, the effect of mutations was consistent across tag positions but not across ligands.

The native degron mutations led to an increase in D_{max} in both tagged cell lines, despite a substantial increase in the steady-state expression of tagged β-catenin. T41A mutation in the internal tag, demonstrated a lower D_{max} compared to the construct without mutations, deviating from other experimental outcomes. It could be hypothesised that the T41A mutation, together with the internal tag, alters the protein's conformation in a way that affects the efficiency of the degradation process (Figure 10a). Further studies are needed to explore these possibilities and therefore further investigation was only performed in C-terminally tagged β-catenin. Treatment with dTAG ligands decreased C-terminally tagged β-catenin to the same absolute level in both S33F mutant and wild-type native degron constructs, despite the former starting at ~ 5-fold higher levels (Figure 9 and 11). This finding indicated that the stabilising effect of these mutations did not impact the maximum degradation achieved by the dTAG system. Instead, data suggested that the production rate of tagged β-catenin rather than stability, could be a critical factor in determining the maximum degradation levels. In the experiment, where protein synthesis was inhibited by CHX and degradation induced with $dTAG^{V}$-1, even short exposure to CHX increased D_{max} (Figure 9c), indicating that production substantially impacted on degradation kinetics by PROTACs. However, prolonged exposure to CHX is not a viable option due to its severe side effects, such as inducing cell death or causing cells to detach, which results in autofluorescence, leading to unreliable flow cytometry results (Kozlova *et al.*, 2020). Additionally, CHX affects overall protein levels and was shown to alter protein degradation pathways (Dai *et al.*, 2013). Therefore, the necessary normalisation was performed to avoid overestimating the impact on D_{max} due to CHX. These limitations highlight the challenge of using CHX to determine protein production effects over extended periods. These findings have important implications for the design of TPD strategies, highlighting the need to consider both the production and degradation mechanisms of target proteins in therapeutic contexts.

Tagging proteins can disrupt normal turnover and functions and cause accumulation, potentially leading to overactivation. The steady-state expression of tagged β-catenin showed accumulation only when stabilising mutations were introduced, with the stabilising effect corresponding to the predicted mutation effect score (Figure 8) (Krishna et al., 2023). This could suggest that these mutations alter the native degron's impact on normal turnover. This was further supported by the GSK3β inhibition

experiment (Figure 12b). Inhibition of GSK3β stabilised and activated C-terminally tagged β-catenin, similar to the effect observed with untagged β-catenin (Cohen and Goedert, 2004). This demonstrated that native degron retained some function and that fused β-catenin underwent turnover via $SCF^{\beta TrCP}$-mediated degradation. Notably, S33F did not undergo further stabilisation, suggesting that this mutation hinders phosphorylation by the destruction complex, and in its absence, exerts no additional effect. Thus, the functionality of the native degron appears to vary with distinct effect mutations, as evidenced by the change in GFP fluorescence at a steady state (Figure 8a-b) and the stabilising impact of GSK3β (Figure 12b).

Previous studies have shown that mutant variants of β-catenin exhibit an extended half-life (He et al., 2021), which aligns with observations of tagged β-catenin in this study (Figure 12a). This consistency supports the conclusion that the introduced mutations enhanced protein stability, leading to a prolonged presence of the stabilised β-catenin variant within the cellular environment. There are only a few articles that consider the stability and half-life of PROTAC targets. Some studies have examined ternary complex stability (Riching *et al.*, 2018; Bartlett and Gilbert, 2022) and used mathematical models to predict the maximum degradation achievable by PROTACs based on the target's half-life (Vetma *et al.*, 2024). The latter studies found a similar pattern: proteins with shorter half-lives were less degraded (i.e., lower D_{max}) than those with longer half-lives, which aligned with my findings for the C-terminal fusion with no mutation that had lower D_{max} than prolonged half-life fusion with the S33F mutation (Figure 9-11).

However, the recovery rate of tagged β-catenin after PROTACs exposure did not align with its half-life. Recovery was observed to be prolonged (only reaching 50% by day 5, Figure 12c), whereas the half-life in the absence of PROTAC ranged from 7-12 hours (Figure 12a). A similar pattern was observed in recent studies, where it was hypothesised that despite washing steps, PROTAC ligands have slow release. Potentially, washout experiments fail to remove intracellular pools of ligand, which continue to bind to E3 ligase at low concentrations with their catalytic substoichiometric mode of action, sustaining the degradation of newly produced protein (Hatoyama et al., 2024; Zhang et al., 2024). Nonetheless, given the extensive cell growth that occurs over multiple days in culture, the size of this effect is remarkable.

β-catenin is crucial for both Wnt signalling and cell adhesion, therefore β-catenin is localised in at least two different pools: one at the cell membrane and another that shuttles between the cytosol and nucleus. Accumulation of tagged β-catenin in the cell-cell junction was observed in immunofluorescence images (Figure 13a), which was consistent with previously recorded functional tags of β-catenin (Ambrosi *et al.*, 2022). However, further confirmation of its binding function is required. The subcellular localisation of tagged β-catenin with and without native degron mutations showed notable accumulation in the cytoplasm and nucleus. This indicated that tagged β-catenin could potentially retain the transcriptional regulatory function (Kim *et al.*, 2019). To confirm the ability of C-terminally tagged β-catenin to regulate transciption, expression of the canonical Wnt pathway target gene Axin2 was investigated using qPCR. The data revealed that the C-terminal tag did not prevent β-catenin from activating Axin2 and therefore the transcription regulation (Figure 13c). This aligned with previous studies showing that C-terminal tagging of β-catenin did not impair its functions (Krieghoff, Behrens and Mayr, 2006; Jamieson, Sharma and Henderson, 2011; Kafri *et al.*, 2016; Ambrosi *et al.*, 2022). Transcription activation was consistent with the mutation effect, where no mutation fusion showed almost no change

compared to cells not expressing a β-catenin transgene, while the stabilising mutations led to a proportional increase. The overexpression of the Wnt gene in proportion to the stabilising mutational effect to some extent mirrored the oncogenic mechanisms (Clevers and Nusse, 2012; Gao *et al.*, 2018). However, the primary purpose of this study was not to produce completely normal functional tagged β-catenin, but to focus on degradation kinetics. Thus, confirming that gene regulation was retained and that the tag did not substantially affect the normal mechanism of turnover was sufficient. To confirm normal functionality of tagged constructs, it would be necessary to endogenously tag the gene in a homozygous manner using a cell line where β-catenin is essential or to generate an endogenously degron-tagged mouse line and check for abnormal developmental phenotypes.

5.1. Conclusion

In this study, the impact of synthetic degron tags at various positions on β-catenin's expression, turnover, and oncogenic mechanisms was investigated. The study utilised a model system with synthetic degron tags and the Flp-In system for stable cell line generation, ensuring consistent expression and comparability. The findings highlighted that the position of the synthetic degron influenced the steady-state expression and degradation kinetics of β-catenin. Also, tag fusion at the C-terminus retained at least some of the normal mechanisms of turnover and transcriptional regulatory functions. Additionally, the study demonstrated that stabilising mutations that increase the steady-state expression of β-catenin did not influence the absolute maximum level to which PROTACs can reduce protein expression. However, they did influence Dmax when this parameter is expressed as a percentage of the relevant vehicle-only control condition, due to the higher expression level at baseline. The rate of protein production plays an important role in determining the absolute maximum level of degradation that can be achieved. The findings contributed to a better understanding of the factors influencing TPD efficacy and suggested that the outcome of PROTAC-based cancer therapy could be influenced by the mechanism of oncogene activation.

5.2. Future Direction

Building on the insights gained from this study, several avenues for future research can further elucidate the importance of protein stability and production in PROTAC strategies. Additionally, employing *in vivo* models could provide a complex and dynamic environment that more closely mimics human physiology, allowing for a more accurate assessment of protein behaviour in living organisms. This approach can uncover how protein stability and production are regulated within the context of whole-body interactions and disease states and the effectiveness of TPD therapies in a clinically relevant setting.

Future studies could also explore proteins stabilised through mechanisms other than degron point mutations, such as repeat expansions and aggregation in neurodegenerative diseases. In conditions like Huntington's disease, amyotrophic lateral sclerosis (ALS), and various forms of dementia, proteins often become abnormally stabilised due to repeat expansions that result in long polyglutamine tracts or other repetitive sequences. These sequences can cause proteins to misfold and aggregate, forming insoluble fibrils or inclusion bodies that are resistant to degradation (Wilson *et al.*, 2023). Investigating how PROTACs and related strategies can be

tailored to target these aggregated proteins could open new therapeutic avenues for neurodegenerative diseases.

6. BIBLIOGRAPHY

Adams, J. (2003) 'The proteasome: Structure, function, and role in the cell', *Cancer Treatment Reviews*, 29(SUPPL. 1), pp. 3–9. doi: 10.1016/S0305-7372(03)00081-1.

AlQahtani, A. D. *et al.* (2019) 'Strategies for the production of long-acting therapeutics and efficient drug delivery for cancer treatment', *Biomedicine and Pharmacotherapy*, 113(January), p. 108750. doi: 10.1016/j.biopha.2019.108750.

Ambrosi, G. *et al.* (2022) 'Allele-specific endogenous tagging and quantitative analysis of β-catenin in colorectal cancer cells', *eLife*, 11, pp. 1–27. doi: 10.7554/eLife.64498.

Banik, S. M. *et al.* (2020) 'Lysosome-targeting chimaeras for degradation of extracellular proteins', *Nature*, 584(7820), pp. 291–297. doi: 10.1038/s41586-020-2545-9.

Bartlett, D. W. and Gilbert, A. M. (2022) 'Translational PK-PD for targeted protein degradation', *Chemical Society Reviews*, pp. 181–200. doi: 10.1039/d2cs00114d.

Békés, M., Langley, D. R. and Crews, C. M. (2022) 'PROTAC targeted protein degraders: the past is prologue', *Nature Reviews Drug Discovery*, 21(3), pp. 181–200. doi: 10.1038/s41573-021-00371-6.

Benet, L. Z. *et al.* (2016) 'BDDCS, the Rule of 5 and Drugability Leslie', *Adv Drug Deliv Rev*, 101(1), pp. 89–98. doi: 10.1016/j.addr.2016.05.007.BDDCS.

Besten, den W. and Lipford, R. (2020) 'Prospecting for Molecular Glues', *Nature Chemical Biology*, 16(11), pp. 1154–1155. doi: 10.1038/s41589-020-0647-1.

Bond, A. G. *et al.* (2021) 'Development of BromoTag: A "bump-and-Hole"-PROTAC System to Induce Potent, Rapid, and Selective Degradation of Tagged Target Proteins', *Journal of Medicinal Chemistry*, 64(20), pp. 15477–15502. doi: 10.1021/acs.jmedchem.1c01532.

Bond, M. J. *et al.* (2020) 'Targeted Degradation of Oncogenic KRASG12Cby VHL-Recruiting PROTACs', *ACS Central Science*, 6(8), pp. 1367–1375. doi: 10.1021/acscentsci.0c00411.

Bondeson, D. P. *et al.* (2022) 'Systematic profiling of conditional degron tag technologies for target validation studies', *Nature Communications*, 13(1). doi: 10.1038/s41467-022-33246-4.

Brüschweiler, R. (2003) 'Efficient RMSD measures for the comparison of two molecular ensembles', *Proteins: Structure, Function and Genetics*, 50(1), pp. 26–34. doi: 10.1002/prot.10250.

Buckley, D. L. *et al.* (2015) 'HaloPROTACS: Use of Small Molecule PROTACs to

Induce Degradation of HaloTag Fusion Proteins', *ACS Chem Biol.*, 10(8), pp. 1831–1837. doi: 10.1021/acschembio.5b00442.HaloPROTACS.

Buetow, L. and Huang, D. T. (2016) 'Structural insights into the catalysis and regulation of E3 ubiquitin ligases', *Nature Reviews Molecular Cell Biology*, 17(10), pp. 626–642. doi: 10.1038/nrm.2016.91.

Che, Y. *et al.* (2018) 'Inducing protein-protein interactions with molecular glues', *Bioorganic and Medicinal Chemistry Letters*, 28(15), pp. 2585–2592. doi: 10.1016/j.bmcl.2018.04.046.

Chen, X., Zaro, J. and Shen, W.-C. (2013) 'Fusion Protein Linkers: Property, Design and Functionality Xiaoying', *Adv Drug Deliv Rev.*, 65(10), pp. 1357–1369. doi: 10.1016/j.addr.2012.09.039.

Ciulli, A. *et al.* (2023) 'The 17th EFMC Short Course on Medicinal Chemistry on Small Molecule Protein Degraders', *ChemMedChem*, 18(20), pp. 1–7. doi: 10.1002/cmdc.202300464.

Clevers, H. (2006) 'Wnt/β-Catenin Signaling in Development and Disease', *Cell*, 127(3), pp. 469–480. doi: 10.1016/j.cell.2006.10.018.

Clevers, H. and Nusse, R. (2012) 'Wnt/β-catenin signaling and disease', *Cell*, 149(6), pp. 1192–1205. doi: 10.1016/j.cell.2012.05.012.

Cohen, P. and Goedert, M. (2004) 'GSK3 inhibitors: Development and therapeutic potential', *Nature Reviews Drug Discovery*, 3(6), pp. 479–487. doi: 10.1038/nrd1415.

Coyote-Maestas, W. *et al.* (2020) 'Targeted insertional mutagenesis libraries for deep domain insertion profiling', *Nucleic Acids Research*, 48(2), pp. 1–14. doi: 10.1093/nar/gkz1110.

Dai, C. L. *et al.* (2013) 'Inhibition of protein synthesis alters protein degradation through activation of protein kinase B (AKT)', *Journal of Biological Chemistry*, 288(33), pp. 23875–23883. doi: 10.1074/jbc.M112.445148.

Ford, M. J. *et al.* (2018) 'A Cell/Cilia Cycle Biosensor for Single-Cell Kinetics Reveals Persistence of Cilia after G1/S Transition Is a General Property in Cells and Mice', *Developmental Cell*, 47(4), pp. 509-523.e5. doi: 10.1016/j.devcel.2018.10.027.

Gao, C. *et al.* (2018) 'Exon 3 mutations of CTNNB1 drive tumorigenesis: A review', *Oncotarget*, 9(4), pp. 5492–5508. doi: 10.18632/oncotarget.23695.

Gerstberger, S., Hafner, M. and Tuschl, T. (2014) 'A census of human RNA-binding proteins', *Nature Reviews Genetics*, 15(12), pp. 829–845. doi: 10.1038/nrg3813.

Gowans, F. A. *et al.* (2024) 'Flor A. Gowans, # Nafsika Forte, # Justin Hatcher, Oscar W. Huang, Yangzhi Wang, Belen E. Altamirano Poblano, Ingrid E. Wertz, and Daniel K. Nomura *'. doi: 10.1021/jacs.4c05174.

Guezguez, B. *et al.* (2016) 'GSK3 Deficiencies in Hematopoietic Stem Cells Initiate Pre-neoplastic State that Is Predictive of Clinical Outcomes of Human Acute

Leukemia', *Cancer Cell*, 29(1), pp. 61–74. doi: 10.1016/j.ccell.2015.11.012.

Hatoyama, Y. *et al.* (2024) 'Combination of AID2 and BromoTag expands the utility of degron-based protein knockdowns', *bioRxiv*, p. 2024.03.20.586026. Available at: https://www.biorxiv.org/content/10.1101/2024.03.20.586026v1%0Ahttps://www.biorxiv.org/content/10.1101/2024.03.20.586026v1.abstract.

He, J. *et al.* (2021) 'Characterization of novel CTNNB1 mutation in Craniopharyngioma by whole-genome sequencing', *Molecular Cancer*, 20(1), pp. 1–16. doi: 10.1186/s12943-021-01468-7.

Hinkson, I. V. and Elias, J. E. (2011) 'The dynamic state of protein turnover: It's about time', *Trends in Cell Biology*, 21(5), pp. 293–303. doi: 10.1016/j.tcb.2011.02.002.

Holdgate, G. A. *et al.* (2023) 'Screening for molecular glues – Challenges and opportunities', *SLAS Discovery*, (November). doi: 10.1016/j.slasd.2023.12.008.

Hou, C. *et al.* (2022) 'Systematic prediction of degrons and E3 ubiquitin ligase binding via deep learning', *BMC Biology*, 20(1), pp. 1–19. doi: 10.1186/s12915-022-01364-6.

Huber, A. H., Nelson, W. J. and Weis, W. I. (1997) 'Three-dimensional structure of the armadillo repeat region of β-catenin', *Cell*, 90(5), pp. 871–882. doi: 10.1016/S0092-8674(00)80352-9.

Huber, L. A. and Teis, D. (2016) 'Lysosomal signaling in control of degradation pathways', *Current Opinion in Cell Biology*, 39, pp. 8–14. doi: 10.1016/j.ceb.2016.01.006.

Jamieson, C., Sharma, M. and Henderson, B. R. (2011) 'Regulation of β-catenin nuclear dynamics by GSK-3β involves a LEF-1 positive feedback loop', *Traffic*, 12(8), pp. 983–999. doi: 10.1111/j.1600-0854.2011.01207.x.

Kafri, P. *et al.* (2016) 'Quantifying β-catenin subcellular dynamics and cyclin D1 mRNA transcription during Wnt signaling in single living cells', *eLife*, 5(NOVEMBER2016), pp. 1–29. doi: 10.7554/eLife.16748.

Kelm, J. M. *et al.* (2023) 'PROTAC'ing oncoproteins: targeted protein degradation for cancer therapy', *Molecular Cancer*, 22(1), pp. 1–43. doi: 10.1186/s12943-022-01707-5.

Kim, W. K. *et al.* (2019) 'B-Catenin Activation Down-Regulates Cell-Cell Junction-Related Genes and Induces Epithelial-To-Mesenchymal Transition in Colorectal Cancers', *Scientific Reports*, 9(1), pp. 1–15. doi: 10.1038/s41598-019-54890-9.

Kostic, M. and Jones, L. H. (2020) 'Critical assessment of targeted protein degradation as a research tool and pharmacological modality', *Trends in Pharmacological Sciences*, 41(5), pp. 305–317. doi: 10.1016/j.tips.2020.02.006.

Kozlova, A. A. *et al.* (2020) 'Changes in Autofluorescence Level of Live and Dead Cells for Mouse Cell Lines', *Journal of Fluorescence*, 30(6), pp. 1483–1489. doi:

10.1007/s10895-020-02611-1.

Kramer, L. T. and Zhang, X. (2022) ‘Expanding the landscape of E3 ligases for targeted protein degradation’, *Current Research in Chemical Biology*, 2, p. 100020. doi: 10.1016/j.crchbi.2022.100020.

Krieghoff, E., Behrens, J. and Mayr, B. (2006) ‘Nucleo-cytoplasmic distribution of β-catenin is regulated by retention’, *Journal of Cell Science*, 119(7), pp. 1453–1463. doi: 10.1242/jcs.02864.

Krishna, A. *et al.* (2023) ‘Mutational scanning reveals oncogenic CTNNB1 mutations have diverse effects on signalling and clinical traits Anagha’, *bioRxiv preprint*. doi: 10.1101/2023.11.09.566307.

Labbadia, J. and Morimoto, R. I. (2015) ‘The biology of proteostasis in aging and disease’, *Annual Review of Biochemistry*, 84, pp. 435–464. doi: 10.1146/annurev-biochem-060614-033955.

Lai, A. C. *et al.* (2016) ‘Modular PROTAC Design for the Degradation of Oncogenic BCR-ABL’, *Angewandte Chemie - International Edition*, 55(2), pp. 807–810. doi: 10.1002/anie.201507634.

Lee, J. M. *et al.* (2023) ‘Control of protein stability by post-translational modifications’, *Nature Communications*, 14(1), pp. 1–16. doi: 10.1038/s41467-023-35795-8.

Li, Z. *et al.* (2020) ‘ATTEC: a potential new approach to target proteinopathies’, *Autophagy*, 16(1), pp. 185–187. doi: 10.1080/15548627.2019.1688556.

Liu, J. *et al.* (2022) ‘Wnt/β-catenin signalling: function, biological mechanisms, and therapeutic opportunities’, *Signal Transduction and Targeted Therapy*, 7(1). doi: 10.1038/s41392-021-00762-6.

Lucas, X. and Ciulli, A. (2017) ‘Recognition of substrate degrons by E3 ubiquitin ligases and modulation by small-molecule mimicry strategies’, *Current Opinion in Structural Biology*, 44, pp. 101–110. doi: 10.1016/j.sbi.2016.12.015.

Macdonald, L. *et al.* (2022) ‘Rapid and specific degradation of endogenous proteins in mouse models using auxin-inducible degrons’, *eLife*, 11, pp. 1–25. doi: 10.7554/eLife.77987.

March, J. C., Rao, G. and Bentley, W. E. (2003) ‘Biotechnological applications of green fluorescent protein’, *Applied Microbiology and Biotechnology*, 62(4), pp. 303–315. doi: 10.1007/s00253-003-1339-y.

Mészáros, B. *et al.* (2017) ‘Degrons in cancer’, *Science Signaling*, 10(470). doi: 10.1126/scisignal.aak9982.

Nabet, B. *et al.* (2018) ‘The dTAG system for immediate and target-specific protein degradation’, *Nature Chemical Biology*, 14(5), pp. 431–441. doi: 10.1038/s41589-018-0021-8.

Nabet, B. *et al.* (2020) ‘Rapid and direct control of target protein levels with VHL-recruiting dTAG molecules’, *Nature Communications*, 11(1). doi: 10.1038/s41467-020-18377-w.

Nadler, D. C. *et al.* (2016) ‘Rapid construction of metabolite biosensors using domain-insertion profiling’, *Nature Communications*, 7. doi: 10.1038/ncomms12266.

Natsume, T. *et al.* (2016) ‘Rapid Protein Depletion in Human Cells by Auxin-Inducible Degron Tagging with Short Homology Donors’, *Cell Reports*, 15(1), pp. 210–218. doi: 10.1016/j.celrep.2016.03.001.

Natsume, T. and Kanemaki, M. T. (2017) ‘Conditional Degrons for Controlling Protein Expression at the Protein Level’, *Annual Review of Genetics*, 51, pp. 83–102. doi: 10.1146/annurev-genet-120116-024656.

Neklesa, T. K., Winkler, J. D. and Crews, C. M. (2017) ‘Targeted protein degradation by PROTACs’, *Pharmacology and Therapeutics*, 174, pp. 138–144. doi: 10.1016/j.pharmthera.2017.02.027.

Pessoa, J. *et al.* (2022) ‘Editorial: Altered Expression of Proteins in Cancer: Function and Potential Therapeutic Targets’, *Frontiers in Oncology*, 12(June), pp. 1–6. doi: 10.3389/fonc.2022.949139.

Rebouissou, S. *et al.* (2016) ‘Genotype-phenotype correlation of CTNNB1 mutations reveals different ß-catenin activity associated with liver tumor progression’, *Hepatology*, 64(6), pp. 2047–2061. doi: 10.1002/hep.28638.

Riching, K. M. *et al.* (2018) ‘Quantitative Live-Cell Kinetic Degradation and Mechanistic Profiling of PROTAC Mode of Action’, *ACS Chemical Biology*, 13(9), pp. 2758–2770. doi: 10.1021/acschembio.8b00692.

Rimm, D. L. *et al.* (1995) ‘α1(E)-catenin is an actin-binding and -bundling protein mediating the attachment of F-actin to the membrane adhesion complex’, *Proceedings of the National Academy of Sciences of the United States of America*, 92(19), pp. 8813–8817. doi: 10.1073/pnas.92.19.8813.

Ross, A. B., Langer, J. D. and Jovanovic, M. (2021) ‘Proteome turnover in the spotlight: Approaches, applications, and perspectives’, *Molecular and Cellular Proteomics*, 20, p. 100016. doi: 10.1074/MCP.R120.002190.

Samarasinghe, K. T. G. and Crews, C. M. (2021) ‘Targeted Protein Degradation: A Promise for Undruggable Proteins’, *Cell Chem Biol*, 28(7), pp. 934–951. doi: 10.1016/j.chembiol.2021.04.011.

Sasso, J. M. *et al.* (2023) ‘Molecular Glues: The Adhesive Connecting Targeted Protein Degradation to the Clinic’, *Biochemistry*, 62(3), pp. 601–623. doi: 10.1021/acs.biochem.2c00245.

Schatoff, E. M. *et al.* (2019) ‘Distinct colorectal cancer–associated apc mutations dictate response to tankyrase inhibition’, *Cancer Discovery*, 9(10), pp. 1358–1371. doi: 10.1158/2159-8290.CD-19-0289.

Simpson, L. M. *et al.* (2020) 'Inducible Degradation of Target Proteins through a Tractable Affinity-Directed Protein Missile System', *Cell Chemical Biology*, 27(9), pp. 1164-1180.e5. doi: 10.1016/j.chembiol.2020.06.013.

Simpson, L. M. *et al.* (2022) 'Target protein localization and its impact on PROTAC-mediated degradation', *Cell Chemical Biology*, 29(10), pp. 1482-1504.e7. doi: 10.1016/j.chembiol.2022.08.004.

Song, J. *et al.* (2023) 'Targeted protein degradation in drug development: Recent advances and future challenges', *European Journal of Medicinal Chemistry*, 261(August), p. 115839. doi: 10.1016/j.ejmech.2023.115839.

Szczesny, R. J. *et al.* (2018) 'Versatile approach for functional analysis of human proteins and efficient stable cell line generation using flp-mediated recombination system', *PLoS ONE*, 13(3), pp. 1–29. doi: 10.1371/journal.pone.0194887.

Tahmasebi, S. *et al.* (2019) 'Protein synthesis and translational control: A historical perspective', *Cold Spring Harbor Perspectives in Biology*, 11(9). doi: 10.1101/cshperspect.a035584.

Tan, X. *et al.* (2007) 'Mechanism of auxin perception by the TIR1 ubiquitin ligase', *Nature*, 446(7136), pp. 640–645. doi: 10.1038/nature05731.

Uitdehaag, J. C. M. *et al.* (2015) 'Selective targeting of CTNNB1-, KRAS- or MYC-Driven cell growth by combinations of existing drugs', *PLoS ONE*, 10(5), pp. 1–22. doi: 10.1371/journal.pone.0125021.

Vetma, V. *et al.* (2024) 'Confounding factors in targeted degradation of short-lived proteins', *bioRxiv*, p. 2024.02.19.581012. Available at: http://biorxiv.org/content/early/2024/02/22/2024.02.19.581012.abstract.

Van Der Wal, T. and Van Amerongen, R. (2020) 'Walking the tight wire between cell adhesion and WNT signalling: A balancing act for β-catenin: A balancing act for CTNNB1', *Open Biology*, 10(12). doi: 10.1098/rsob.200267.

Wilson, D. M. *et al.* (2023) 'Hallmarks of neurodegenerative diseases', *Cell*, 186(4), pp. 693–714. doi: 10.1016/j.cell.2022.12.032.

Wu, G. *et al.* (2003) 'Structure of a β-TrCP1-Skp1-β-catenin complex: Destruction motif binding and lysine specificity of the SCFβ-TrCP1 ubiquitin ligase', *Molecular Cell*, 11(6), pp. 1445–1456. doi: 10.1016/S1097-2765(03)00234-X.

Wu, T. *et al.* (2020) 'Targeted protein degradation as a powerful research tool in basic biology and drug target discovery', *Nature Structural and Molecular Biology*, 27(7), pp. 605–614. doi: 10.1038/s41594-020-0438-0.

Xing, Y. *et al.* (2008) 'Crystal Structure of a Full-Length β -Catenin', *Structure*, 16(3), pp. 478–487. doi: 10.1016/j.str.2007.12.021.

Xu, H., Hu, R. and Zhao, Z. (2023) 'DegronMD: Leveraging Evolutionary and Structural Features for Deciphering Protein-Targeted Degradation, Mutations, and Drug Response to Degrons', *Molecular Biology and Evolution*, 40(12), pp. 1–11. doi:

10.1093/molbev/msad253.

Yardy, G. W. *et al.* (2009) 'Mutations in the AXIN1 Gene in Advanced Prostate Cancer', *European Urology*, 56(3), pp. 486–494. doi: 10.1016/j.eururo.2008.05.029.

Zeng, M. *et al.* (2020) 'Exploring Targeted Degradation Strategy for Oncogenic KRASG12C', *Cell Chemical Biology*, 27(1), pp. 19-31.e6. doi: 10.1016/j.chembiol.2019.12.006.

Zhang, D. *et al.* (2024) 'Tissue distribution and retention drives ef fi cacy of rapidly clearing VHL-based PROTACs', 5. doi: 10.1038/s43856-024-00505-y.

Zhang, X. *et al.* (2019) 'Electrophilic PROTACs that degrade nuclear proteins by engaging DCAF16', *Nature Chemical Biology*, 15(7), pp. 737–746. doi: 10.1038/s41589-019-0279-5.

Zordan, R. E. *et al.* (2015) 'Avoiding the ends: Internal epitope tagging of proteins using transposon Tn7', *Genetics*, 200(1), pp. 47–58. doi: 10.1534/genetics.114.169482.

Zou, Y., Ma, D. and Wang, Y. (2019) 'The PROTAC technology in drug development', *Cell Biochemistry and Function*, 37(1), pp. 21–30. doi: 10.1002/cbf.3369.